



Universida de Vigo



Universidad  
Carlos III de Madrid



POLITÉCNICA

Máster en Matemática Industrial

Curso 2015/16

Trabajo Fin de Máster

# Low-Rank Reconstruction in Non-Uniform Sampling NMR

David Orive Miguel

**Fecha presentación:** 18-07-2016  
**Tutor académico:** Iñigo Arregui Álvarez  
**Empresa:** Mestrelab Research  
**Tutor empresa:** Santiago López Ponte





## Resumen

Durante el último medio siglo se ha demostrado la utilidad de la espectroscopía de resonancia magnética nuclear para investigar las características de las moléculas orgánicas. Sin embargo, esta técnica es poco sensible, además de necesitar altos tiempos de adquisición para obtener espectros de alta resolución. Por esta razón, en la última década se ha propuesto el muestreo no uniforme para superar los problemas relacionados con el tiempo de adquisición. Aún así, esta técnica de muestreo también tiene desventajas secundarias, como la imposibilidad de utilizar exitosamente la transformada de Fourier para obtener el espectro o la necesidad de introducir algunas hipótesis relativas a la señal. En consecuencia, en la literatura científica se han desarrollado numerosos métodos para superar estos problemas secundarios y poder reconstruir el espectro de una espectroscopía de resonancia magnética nuclear muestreada no uniformemente.

En este trabajo de máster se analiza el rendimiento de un algoritmo, recientemente propuesto, para la reconstrucción de rango bajo de señales de espectroscopía de resonancia magnética nuclear. Además, se propone un método novedoso basado en un híbrido entre las técnicas de muestreo con compresión y de rango bajo. También se estudia la implementación para asegurar su aplicabilidad en ámbitos industriales. En lo relativo a los resultados obtenidos, se concluye que se obtiene una mejora significativa utilizando tanto el algoritmo de rango bajo como el método híbrido con los parámetros óptimos. Finalmente, también se muestra que el método de rango bajo no decrementa significativamente la resolución del espectro reconstruido.

## Abstract

During the last half-century it has been shown the usefulness of nuclear magnetic resonance spectroscopy to investigate the characteristics of organic molecules. Nevertheless, this technique suffers from its low sensitivity and the large acquisition time needed to obtain high resolution spectra. For that reason, in the last decade non-uniform sampling has been proposed to overcome acquisition time problem. However, this sampling technique also involves several secondary drawbacks such as the impossibility of using successfully the Fourier transform to obtain the spectrum of a signal or the necessity to introduce some assumptions about the signal. In consequence, many methods have been developed in the last years to overtake these secondary issues by reconstructing a nuclear magnetic resonance spectroscopy signal from a non-uniform sampling.

In this master's thesis the performance of a recently proposed low-rank reconstruction algorithm for nuclear magnetic resonance spectroscopy spectra is analyzed. Moreover, a novel method based on an hybrid between compressed sensing and low-rank algorithms is proposed. The implementation in order to ensure its applicability to the industry is also studied. Regarding the obtained results, it is concluded that a significant improvement is obtained when using both the low-rank and the hybrid method with optimal parameters. Finally, it is also shown that the low-rank algorithm does not decrease significantly the resolution of the reconstructed spectrum.



# Contents

<b>Acknowledgments</b>	<b>vii</b>
<b>1 Introduction</b>	<b>1</b>
1.1 Master's Thesis Objectives . . . . .	2
1.2 Mestrelab Research . . . . .	2
1.3 Master's Thesis Structure . . . . .	3
<b>2 Background</b>	<b>5</b>
2.1 Nuclear Magnetic Resonance Spectroscopy . . . . .	5
2.1.1 The Physics of NMR Spectroscopy . . . . .	6
2.1.2 Phase-Acquire Experiment . . . . .	8
2.1.3 Two-Dimensional NMR Spectroscopy . . . . .	9
2.2 Some Notes About Digital Signal Processing . . . . .	11
2.2.1 Noise, Sensitivity and Dynamic Range . . . . .	13
2.2.2 Resolution . . . . .	14
2.3 NMR Spectroscopy Signal Reconstruction Problem . . . . .	16
2.3.1 Reconstruction as a Deconvolution Problem . . . . .	17
2.3.2 Reconstruction as an Optimization Problem . . . . .	18
2.4 Literature Survey . . . . .	22
<b>3 Methodology</b>	<b>25</b>
3.1 Non-Uniform Sampling and Poisson-Gap . . . . .	25
3.1.1 Advantages of Applying Non-Uniform Sampling to Multidimensional Spectrum . . . . .	26
3.2 Optimization Techniques . . . . .	26
3.2.1 Dual Ascent . . . . .	27
3.2.2 Dual Decomposition . . . . .	28
3.2.3 Augmented Lagrangian and Methods of Multipliers . . . . .	29
3.2.4 Alternating Direction Method of Multipliers . . . . .	30
3.2.5 Application of ADMM to the Reconstruction Problem Using Low-Rank Method . . . . .	31

3.2.6	Application of ADMM to the Reconstruction Problem Using Hybrid Method . . . . .	32
3.3	Algorithms Implementation . . . . .	33
3.4	Datasets . . . . .	34
<b>4</b>	<b>Results and Discussion</b>	<b>37</b>
4.1	Comparison between Low-Rank, Compressed Sensing and Hybrid Algorithms . . . . .	37
4.1.1	Spectra Accuracy Comparison . . . . .	37
4.1.2	Computing Time Comparison . . . . .	38
4.1.3	Brief Discussion about the Algorithms . . . . .	38
4.2	Low-Rank Parameters Analysis . . . . .	39
4.3	Differences in Peaks Area between Original and Low-Rank Reconstructed Spectrum . . . . .	42
4.4	Resolution of Low-Rank Reconstructed Spectrum . . . . .	45
4.5	Some Notes about Results Randomness Produced by Poisson-Gap Sampling . . . . .	46
<b>5</b>	<b>Conclusions and Future Work</b>	<b>51</b>

# List of Figures

2.1	Larmor precession and its projection. . . . .	8
2.2	Example of a free induction decay signal. . . . .	8
2.3	First vertical black line is the pulse of the preparation step, then evolution takes place, second black line represents the pulses of the mixing period and finally the detection time happens. . . . .	9
2.4	Data structure for a typical two-dimensional experiment. Each row is a one-dimensional free induction decay signal and $\Delta_1$ and $\Delta_2$ are time intervals for indirect and direct time respectively. . . . .	10
2.5	In the left figure low sampling frequency is done (less dots can be seen) and in the right one higher sampling frequency is used; however, in both of them same measuring time is needed. So, it is proved that higher resolution in direct time $t_2$ does not imply to spend more time. . . . .	11
2.6	In the left image an experiment by using $\Delta_1$ time interval can be seen, in this case two FIDs signals were recorded. In the right image the time interval is $\Delta_1^* = \Delta_1/2$ so better resolution will be obtained but twice experiments must be done. It can be seen that an increase in indirect time resolution implies an increase in the number of signals to be recorded and therefore to perform a whole experiment will take much more time. . . . .	12
2.7	First example of a Fourier grid. The separation between each dot is uniform so if all points are sampled then US is performed. However, if only black dots (usually randomly selected) are sampled then it is called NUS sampling and as it can be seen distance between each black point is not uniform. Image taken from [25]. . . . .	13
2.8	Second example of a Fourier grid. It is shown that non-uniform sampling is equivalent to applying the Fourier grid but not taking all samples. Image taken from [19]. . . . .	13
2.9	Example of signal ambiguity that happens if the sampling frequency is not the adequate, known as <i>aliasing</i> . . . . .	14

- 2.10 In picture *a* and *c* the original signal and a set of delta functions separated by  $1/f_s$  are shown respectively. Its Fourier transforms are shown in pictures *b* and *d*, it should be noted that now the set of Delta functions are separated by  $f_s$ . The discretized signal which is just the multiplication of *a* and *c* is plotted in picture *e*. Finally, the spectrum of the discretized signal which is equivalent to do the convolution of the spectrum of the original signal and the set of Delta functions is shown in picture *f*. As it can be seen, copies of the original spectrum occur, the reason is clear when considering the convolution of the original spectrum and the set of Delta functions.  
Image taken from [38]. . . . . 15
- 2.11 It is shown what happens by using different sampling frequencies. If  $f_s > 2B$  then copies of the spectrum are more separated between them, if  $f_s = 2B$  then there is no separation and if  $f_s < 2B$  then copies of the spectra overlap each other and aliasing occurs. Image taken from [38]. . . . . 16
- 2.12 The left and right images are examples of a spectrum with low and high resolution respectively. As it can be seen, when a spectrum has low resolution then two near peaks will overlap and they will appear as just one big peak. . . . . 17
- 2.13 The top row shows data in the time domain and the bottom row shows the DFT of the top row data. The left column shows uniformly sampled signal and its DFT. In the central column a random sampling schedule can be seen (with 0's and 1's) and its DFT which is a *point spread function* (PSF) in the frequency domain. The right column shows the DFT of the signal non-uniformly sampled. The figure demonstrates that multiplying the time domain of a signal by a sampling schedule and doing its DFT is equivalent to do the convolution of the frequency domain spectrum with the point spread function, that is,  $DFT(a \times b) = DFT(c) = DFT(a) \otimes DFT(b) = d \otimes e = f$ . Note that the convolved signal intensity has decreased due to PSF maximum intensity is less than one. . . . . 19
- 3.1 Example of applying US and NUS to a two-dimensional signal where  $t_1$  is the indirect dimension and  $t_2$  is the direct dimension. It should be noted that when using NUS less signals are sampled. Images taken from [19]. . . . . 26
- 3.2 HSQC NMR bidimensional spectrum from where experimental signals were taken from. . . . . 35

3.3	DFT of the experimental signals that were used in the analysis; blue and green lines correspond to real and imaginary parts of the spectrum respectively. It can be seen that last five signals are just noise. . . . .	36
4.1	Synthetic signals used for the experiments with different Gaussian noise. . . . .	39
4.2	$L^2$ relative error for synthetic data with a fixed NUS ratio of 0.2 by using different $\lambda$ and Gaussian noise standard deviation values. . . . .	40
4.3	$L^2$ relative error for synthetic data with $\lambda = 10$ by using different NUS ratio and Gaussian noise standard deviation values. . . . .	40
4.4	$L^2$ relative error for experimental data by using different $\lambda$ values and a fixed NUS ratio of 0.2. . . . .	41
4.5	$L^2$ error for experimental data by using different NUS values and $\lambda = 10$ . . . . .	41
4.6	First pack of signals. Real (blue) and imaginary (green) parts of the spectrum from experimental signals. Each row is a different signal and columns (from left to right) are the original and reconstructed spectra with NUS ratio equal to 0.2, 0.4 and 0.6. . . . .	43
4.7	Second pack of signals. Real (blue) and imaginary (green) parts of the spectrum from experimental signals with noise. Each row is a different signal and columns (from left to right) are the original and reconstructed spectra with NUS ratio equal to 0.2, 0.4 and 0.6. . . . .	44
4.8	2D spectra with two intensity thresholds from where experimental signals were taken. Blue dots indicate high content of noise. . . . .	45
4.9	Example of peak segmentation where yellow line is the maximum height of the peak, red line is the width at half maximum height and green line is the considered domain of the peak which is five times the red line. . . . .	46
4.10	In the upper image the original synthetic spectrum can be seen where numbering of peaks is done from left to right and the area of peaks is also in increasing order from left to right. In the lower images it is shown peak area relative error for different standard deviation Gaussian noise ( $\sigma = 0.3, 0.5, 0.7$ ) and several $\lambda$ values are shown. Minimal error is obtained for $\lambda$ values greater than 10. . . . .	47
4.11	Real (blue) and imaginary (green) parts of the spectrum from resolution experiment. Each row is a different signal with frequencies at different points but with same amplitude and decaying rate. Columns (from left to right) are the original and reconstructed spectrum with NUS ratio equal to 0.2, 0.4 and 0.6. . . . .	48



# Acknowledgments

Now, it is time to take a look back and realize about all the new things I have learned during this master's degree. I still remember when I took the first lectures and I acknowledged that I did not understand many of the concepts and contexts that were explained due to my lack of experience in the field of applied mathematics. In that moment I realized that I was in the right place because I wanted to face a new and exciting challenge. As a consequence, during this master's degree I have learned a lot of applied mathematics and physics concepts that I was willing to achieve. For these reasons, I think that I took the right decision when I chose this master's degree.

Regarding this thesis, I have to say that it has been an exciting topic from which I have learned many interesting concepts and applications that will be useful for my future professional and academic career. I would like to thank everyone who made it possible: my industrial tutor Santiago López Ponte (Mestrelab) and specially my academic tutor Iñigo Arregui Álvarez for all his support and suggestions during this project.

Last but not least, I would like to say that I am enormously grateful to my parents and brother for their support along this long journey away from home.

David Orive Miguel

July, 2016  
Santiago de Compostela



# Chapter 1

## Introduction

Nuclear magnetic resonance spectroscopy is a broadly used research technique among chemists in order to investigate the characteristics of organic molecules. Since its development in 40's and 50's by Purcell and Bloch groups it has been improved not only concerning the used experimental equipment but also in its data processing. Now, it is widely used in biochemistry laboratories and a large amount of successful results are being published. However, nuclear magnetic resonance spectroscopy suffers from some drawbacks such as the lack of sensitivity and the necessity to wait for long times to acquire a high resolution signal (mainly in multidimensional signals). These difficulties can diminish interesting experiments for certain molecules.

This master's thesis focuses on the second problem that is commonly found in the laboratories. The problem can be described as follows: in order to obtain a high quality multidimensional spectrum it is necessary to sample a lot of signals at high resolution. Usually, signals are sampled at uniform time intervals; however the smaller the interval the better the resolution but the more time it takes. In the last decade, sampling of the signals at non-uniform intervals -with less samples than in the uniform sampling- has become a popular technique to minimize the previous problem. The main advantage is that performing an experiment takes less time and therefore experimenters obtain results faster. Nevertheless, taking fewer points at non-uniform intervals make things much more complex. First, spectrum of the signal cannot be obtained directly by using Fourier transform; not sampled points of the signal must be reconstructed. Second, some assumptions about the signal must be introduced in order to perform a successful reconstruction. In order to overcome these disadvantages, novel methods should be developed so as to provide better quality signal to chemists. In the last years several methods that try to solve these problems have been published; one of them is the compressed sensing algorithm [30] which was previously used in astronomy. A recent published technique is the low-rank algorithm [42], which shows promising results.

In this master's thesis the performance of the low-rank algorithm for the reconstruction of nuclear magnetic resonance spectroscopy data is analyzed. Special emphasis is done in the study of the algorithm performance under different parameter values. The performed experiments are validated both using synthetic and experimental data provided by Mestrelab Research industrial partner. Moreover, a novel method -based on compressed sensing and low-rank algorithms- is proposed; however, due to planning reasons its capabilities have not been fully analyzed.

## 1.1 Master's Thesis Objectives

The objectives of this master's thesis are the following:

- To analyze the performance of the low-rank algorithm described in [42] under different conditions.
- To investigate its applicability and viability to solve industrial problems encountered by Mestrelab industrial company.
- To consider low-rank algorithm optimal implementation approaches so as to make it a fast algorithm and practical for the industry.
- Eventually, to propose a new algorithm that could perform better reconstructions in some situations.

## 1.2 Mestrelab Research

Mestrelab Research is the company that proposed the problem that is going to be analyzed in this master's thesis. They develop software to analyze and process data from nuclear magnetic resonance and mass spectroscopy. *Mnova* software is their main product and is commonly used in analytical and organic chemistry. For these reasons, Mestrelab is interested in researching under what conditions the performance of low-rank reconstruction algorithm is optimal.

Mestrelab Research was founded 11 years ago in Santiago de Compostela (Spain). It has around 26 employees, 21 of which are working in Santiago de Compostela and 5 are collaborating from United Kingdom and United States.

Their software can be divided in two key sections: the first part is focused on nuclear magnetic resonance spectroscopy and the software is able to process data obtained from different spectrometer brands such as *Agilent*, *Bruker*, *JEOL*, *PicoSpin*, *Magritek*, *Nanalysis* or *Oxford Instruments*. The data processing is automatic and has several tools for the analysis of the spectral signal. The other part of their software is dedicated to the processing of mass spectroscopy data that

allows chemists obtaining information about the chemical structure of molecules. Both products are multiplatform, are updated periodically and allow plugins purchasing to add new functionalities. Mestrelab Research also offers user support, the software is correctly documented and there exists a large amount of video-tutorials to learn how to use the software.

## 1.3 Master's Thesis Structure

The chapters included in this thesis are described below:

- **Background:** In this chapter the reader is introduced to the nuclear magnetic resonance physics and mathematics. In addition, some concepts of digital signal processing are briefly described. Moreover, the concept of non-uniform sampling and its relationship with the nuclear magnetic resonance spectra reconstruction problem is explained. Then, the reconstruction problems are posed as optimization problems based on compressed sensing, low-rank and a novel hybrid method. Finally, the state of the art of the problem is described by reviewing the recent literature.
- **Methodology:** This chapter describes the optimization tools used and how to apply them to solve the posed problems; it is composed of four key sections. In the first section Poisson gap sampling method is described. Then, optimization techniques are analyzed as the solution to the reconstruction problems posed in the first chapter. In the next section, the previously described optimization techniques are applied to the reconstruction problems. Finally, implementation details for the low-rank and hybrid method are discussed.
- **Results and Discussion:** In the first part of this chapter the low-rank, compressed sensing and hybrid algorithm are compared in terms of reconstruction accuracy and computational time. Then, after justifying low-rank algorithm as the most efficient algorithm overall, its performance is analyzed under different conditions. Moreover, an useful discussion is maintained about the obtained results and its implications to the industrial application of low-rank algorithm.
- **Conclusions and Future Work:** In the last chapter the key conclusions of the master's thesis are summarized and their utility for the industry is discussed. Finally, the work that could be done to continue the research initiated in this thesis is briefly sketched.



# Chapter 2

## Background

The goal of this chapter is giving to the reader a basic background knowledge so as to understand the context surrounding the project and its importance. First, basic background on the field of nuclear magnetic resonance spectroscopy and signal processing will be explained. Moreover, an introduction to the problem of recovering a free induction decay signal from a non-uniform sampling will be given. Finally, the current state-of-the-art of nuclear magnetic resonance spectra reconstruction will be analyzed.

### 2.1 Nuclear Magnetic Resonance Spectroscopy

Nuclear Magnetic Resonance spectroscopy, also known as NMR spectroscopy, is a method developed independently by Purcell [41] and Bloch [4] in the middle of the last century, based on magnetic properties of certain atomic nuclei. This technique is useful to determine the physical and chemical properties -such as structure, dynamics or reaction state of atoms and several molecules- of substances. Moreover, it is not destructive and samples weighing less than a milligram can be used. Most commonly used by chemists to research the properties of organic molecules, this technique revolutionized scientific world and nowadays chemistry cannot be imagined without it. For a further introduction to the history of NMR spectroscopy see [17].

In next section, physics and mathematics of NMR spectroscopy will be discussed. Then, the widely known phase-acquire experiment will be described and a brief introduction will be given to two-dimensional NMR spectroscopy.

### 2.1.1 The Physics of NMR Spectroscopy

The nuclei of many elemental isotopes (elements with different number of neutrons) have a characteristic spin such as  $1/2$ ,  $3/2$ ,  $4$  or  $7/2$ ; in this explanation only  $1/2$  spins will be considered although the concepts can be easily applied to other spin numbers. A spinning charge generates a magnetic field, thus, it has a magnetic moment ( $\mu$ ) proportional to the spin. In the presence of an external magnetic field ( $B_0$ ) two spin states ( $+1/2$  and  $-1/2$ ) exist, the former being the one with the lowest energy and the latter the one with the highest energy. The magnetic moment with  $+1/2$  state is aligned with the external field, while the charge with spin state  $-1/2$  points in the opposite direction. In a NMR spectroscopy experiment a lot of nuclei (around  $10^{20}$ ) are contained in a sample. However, the determinant parameter is not the magnitude moment of each nucleus but the net magnetic moment of the sample. If the magnetic moment of each nucleus points in random direction then no net magnetic moment will arise because they cancel out. However, if all magnetic moments point in the same direction then all contributions will be added up and a net magnetic moment will happen. This is known as *bulk magnetization*.

Magnetization is usually represented by a magnetization vector which, for convention, will be directed along the direction of the magnetic field, i.e.,  $z$  axis using a *right-handed set*. If, somehow, the magnetization vector is moved away from the  $z$  axis then the vector will rotate about the axis with constant angle as shown in Figure 2.1a. The vector is said to precess about the field and it is known as *Larmor precession*. The frequency of the Larmor precession is determined by

$$\omega_0 = -\gamma B_0, \text{ (rad s}^{-1}\text{)} \quad (2.1)$$

where  $\gamma$  is the gyromagnetic ratio ( $\text{rad s}^{-1}\text{T}^{-1}$ ) and  $B_0$  (T) is the external applied magnetic field. It should be noted that the gyromagnetic ratio depends on the nucleus, so different samples will have different gyromagnetic ratio values and therefore different Larmor frequencies. As time advances, magnetization has a tendency to return to its equilibrium position on the  $z$  axis, this process is called *relaxation*.

The detection of precession of the magnetic vector is the goal of NMR spectroscopy experiments. In order to digitally record precession the sample is covered with a coil which is aligned with the  $x - y$  plane. Then, when magnetization vector passes above the coil a current is induced which is amplified and generates a signal known as *free induction decay* (FID) signal. This signal can be derived mathematically by considering that the magnetization vector has magnitude  $M_0$  and is separated by a  $\beta$  angle from the  $z$  axis. Its projection on the  $x - y$  plane is defined by  $M_0 \sin \beta$  so the  $x - y$  components of the vector along time are defined

by

$$\begin{cases} S_x &= S_0 \cos(\omega_0 t) \\ S_y &= S_0 \sin(\omega_0 t) \end{cases} \quad (2.2)$$

where  $S_0 \propto M_0 \sin \beta$  is the proportionality constant depending on several instrumental factors and  $\omega_0$  is the Larmor frequency defined in rad s<sup>-1</sup> (see Figure 2.1b). These two components can be described together in a complex signal as

$$\begin{aligned} S(t) &= S_x(t) + iS_y(t) \\ &= S_0 \cos(\omega_0 t) + iS_0 \sin(\omega_0 t) \\ &= S_0 \exp(i\omega_0 t). \end{aligned} \quad (2.3)$$

As the time advances, the magnetization vector tends to recover to the  $z$  axis due to the relaxation process; thus, a decaying exponential must be introduced:

$$S(t) = S_0 \exp(i\omega_0 t) \exp(-t/\tau), \quad (2.4)$$

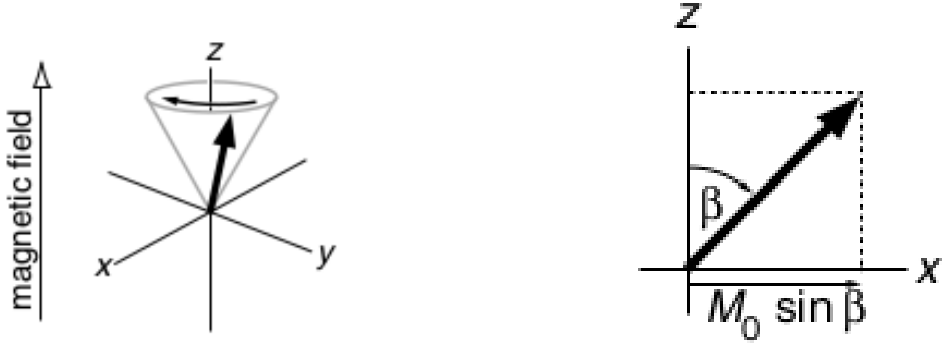
where  $\tau$  is a decaying time constant. If there are several frequency lines in the spectrum due to a sample with  $J$  different spins, then:

$$S(t) = \sum_{j=1}^J S_j \exp(i\omega_j y) \exp(-t/\tau_j). \quad (2.5)$$

Moreover, in order to allow phase shift a phase term is added

$$S(t) = \sum_{j=1}^J S_j \exp(i\omega_j y) \exp(i\phi) \exp(-t/\tau_j). \quad (2.6)$$

Thus,  $S(t)$  is a mathematical expression for free induction decay signal. A classical signal can be seen in Figure 2.2.



(a) Larmor frequency, magnetization vector precesses around the  $z$  axis.

(b) Projection of the magnetization vector into the  $x - y$  plane.

Figure 2.1: Larmor precession and its projection.

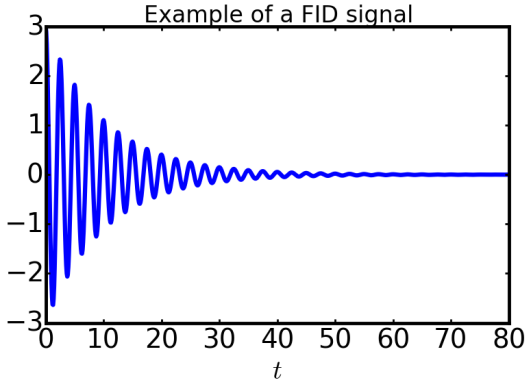


Figure 2.2: Example of a free induction decay signal.

### 2.1.2 Phase-Acquire Experiment

Several types of experiments can be carried out in order to induce precession in a sample. Phase-acquire experiment is the most common way to record one-dimensional spectra of molecules and is based on the previously described physics. The typical steps to be carried out are the following:

1. Sample is allowed to reach equilibrium, that is, the bulk magnetization is directed along the external magnetic field direction.
2. Magnetization vector is perturbed from its equilibrium position by a 90 degrees rotation. Usually, this is done by feeding some radiofrequency power

to the same coil that records the FID signal, which will generate a oscillating magnetic field in the  $x$  direction that must be resonant with the Larmor frequency. That way the magnetization will rotate away from the  $z$  direction even in the presence of the applied strong external magnetic field.

3. Once the radiofrequency power is stopped, the magnetization will start rotating at Larmor frequency and finally will converge to its equilibrium position.

### 2.1.3 Two-Dimensional NMR Spectroscopy

One-dimensional experiments are useful for basic samples. Nevertheless, when dealing with complex and large molecules, signals overlap in a strong way and 1-D experiments are no longer useful. For that reason, two-dimensional experiments have the advantage of removing peaks overlapping and can be used to prove specific NMR interactions selectively. Jean Jeener was the first scientist to develop the theoretical framework for two-dimensional experiments in 1971 during a conference in former Yugoslavia [27]. Thereafter, the experiment was implemented in 1976 by W.P. Aue, E. Bartholdi and R.R. Ernst [2].

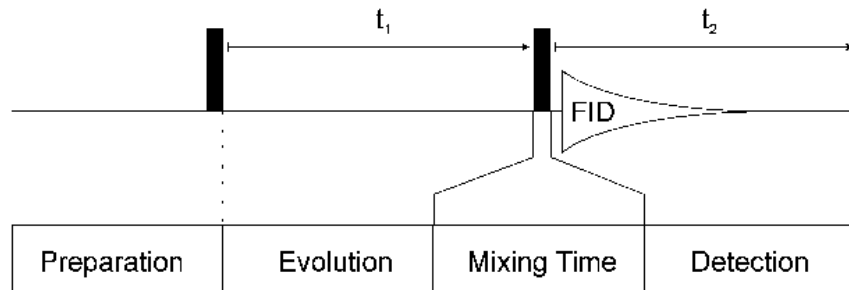


Figure 2.3: First vertical black line is the pulse of the preparation step, then evolution takes place, second black line represents the pulses of the mixing period and finally the detection time happens.

A typical 2D NMR spectroscopy experiment consists on four steps (see Figure 2.3):

- Preparation: The system is prepared in a suitable initial state where magnetization coherence is created through a set of radio frequency pulses.
- Evolution: This step takes  $t_1$  seconds (indirect time), no pulses are generated and the nuclear spins are allowed to freely precess.

- Mixing: Coherence is manipulated by another series of pulses and samples are allowed to interact.
- Detection: Typical one-dimensional FID signal is generated and recorded; it takes  $t_2$  seconds (direct time).

Thus, two-dimensional experiments are a simple series of one-dimensional experiments collected with different evolution timing. Therefore, in a two-dimensional experiment FID signals can be organized in matrix form as shown in Figure 2.4 where each row represents a recorded signal by using different evolution times. By performing a two dimensional FFT on this matrix, a two dimensional frequency spectrum is obtained.

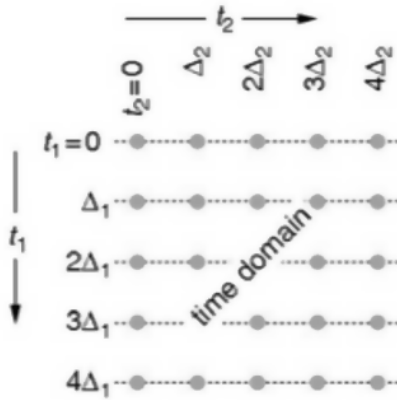


Figure 2.4: Data structure for a typical two-dimensional experiment. Each row is a one-dimensional free induction decay signal and  $\Delta_1$  and  $\Delta_2$  are time intervals for indirect and direct time respectively.

It is important to remark the fact that higher resolution in  $t_2$  (direct time) takes no more time, in fact it is only needed to increase the sampling frequency and the recording of FID signal will always take the same amount of seconds, see Figure 2.5. However, higher resolution in indirect time  $t_1$  adds directly to the total number of one-dimensional experiments to be done, i.e., if resolution is increased by reducing to the half the time interval in  $t_1$  then it will be needed to perform twice one-dimensional records to perform the whole experiment, see Figure 2.6. The implication of this property is the main reason for using non-uniform sampling when performing multidimensional experiments. It will be extensively analyzed in the next section and in Chapter 3.

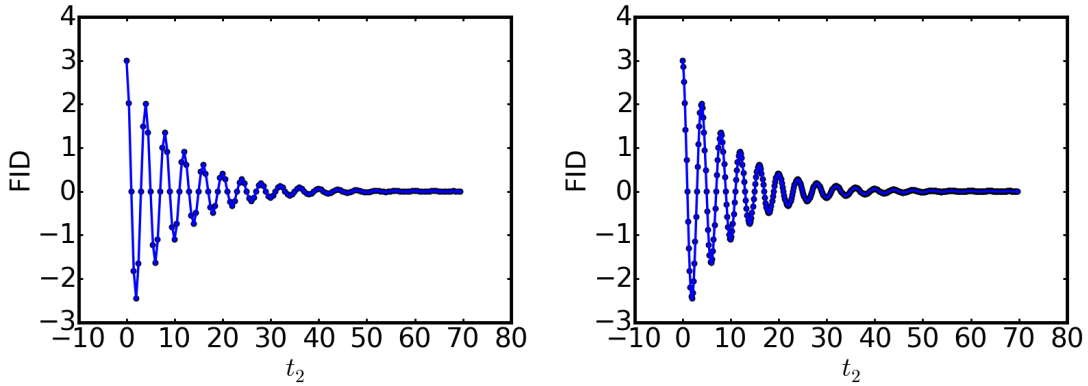


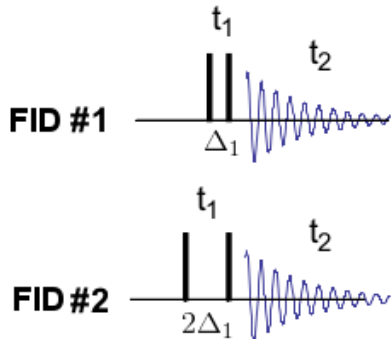
Figure 2.5: In the left figure low sampling frequency is done (less dots can be seen) and in the right one higher sampling frequency is used; however, in both of them same measuring time is needed. So, it is proved that higher resolution in direct time  $t_2$  does not imply to spend more time.

## 2.2 Some Notes About Digital Signal Processing

Digital Signal Processing (DSP) is a fundamental cornerstone of NMR spectroscopy as it deals with the conversion of analog signals to digital and the computational processing of the latter. In NMR spectroscopy the FID signals contain information about the analyzed sample so a good processing could retrieve valuable information. When performing DSP on a FID signal the first step is the discretization, i.e., taking samples from the FID analog signal. The most important part when performing sampling is to decide the sampling frequency, i.e. the interval time between each sample which can be taken at constant or random times, which are called uniform (US) and non-uniform sampling (NUS) respectively. In this work, NUS denotes the random taking of samples from a uniform grid, that is, when doing US what is done is to create a *Fourier grid* with uniform separations between samples and when doing NUS random points from that grid are taken so spaces between selected points are not uniform. It should be noted that when performing NUS less points are always taken than when doing US, (see Figures 2.7 and 2.8).

Sampling is not such a naïve task as it might seem because several problems can arise. For example, if the US frequency is too low then several frequencies could have produced the sampled data; this is shown in Figure 2.9, where the green dots are the points sampled by a US frequency of 6kHz and the sampled dots could have been produced both by a 7kHz and 1kHz signal. Thus, ambiguity arises as it is not known which signal produced each sample; this is known as *aliasing*. The starting point to understand this phenomenon and to avoid it is by taking into account the Nyquist Criterion also known as the Shannon Sampling Theorem which states that *given a signal with a maximum frequency  $B$  then the sampling frequency must*

## Experiment #1



## Experiment #2

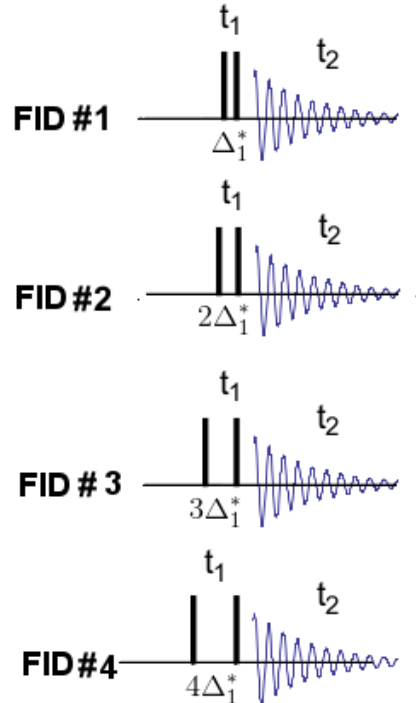


Figure 2.6: In the left image an experiment by using  $\Delta_1$  time interval can be seen, in this case two FIDs signals were recorded. In the right image the time interval is  $\Delta_1^* = \Delta_1/2$  so better resolution will be obtained but twice experiments must be done. It can be seen that an increase in indirect time resolution implies an increase in the number of signals to be recorded and therefore to perform a whole experiment will take much more time.

be greater than  $2B$  in order to reproduce the periodic signal without ambiguity.

The previous problem can also be understood by realizing that digitalizing a signal in the time domain is equivalent to multiplying it by several Dirac delta functions separated by  $1/f_s$ , where  $f_s$  is the sampling frequency. Replications of the original spectrum must occur in the obtained spectrum as can be seen graphically in Figure 2.10 because the convolution theorem [1] states that doing the Fourier transform (conversion from time domain to the frequency domain) of a product between two signals is equivalent to the convolution of the Fourier transform of each signal.

When the sampling frequency,  $f_s$ , is less than  $2B$  ( $B$  being the maximum frequency of the original signal) then spectra replications collapse and aliasing occurs, as it is shown in Figure 2.11.

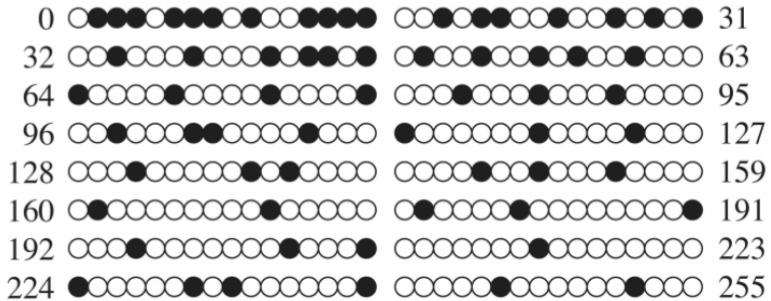


Figure 2.7: First example of a Fourier grid. The separation between each dot is uniform so if all points are sampled then US is performed. However, if only black dots (usually randomly selected) are sampled then it is called NUS sampling and as it can be seen distance between each black point is not uniform. Image taken from [25].

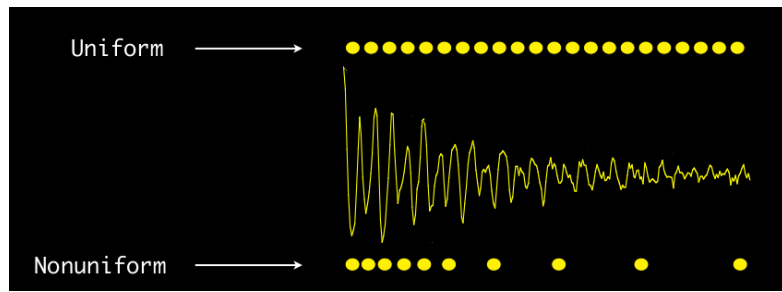


Figure 2.8: Second example of a Fourier grid. It is shown that non-uniform sampling is equivalent to applying the Fourier grid but not taking all samples. Image taken from [19].

### 2.2.1 Noise, Sensitivity and Dynamic Range

When assessing the quality of a NMR signal the terms of noise and dynamic range are very important. The first occurs in the registering of FID signal, some part of this noise comes from amplifiers and other electronics devices of the spectrometer, but the major contribution is given by the thermal noise from the detection coil. In order to measure the relationship between signal and noise, the *sensitivity* is used; it is defined as the minimum quantity of signal that can be distinguished from noise. To measure it, a *signal to noise ratio* (SNR) is usually used; it is defined by:

$$SNR = \frac{P_{signal}}{P_{noise}}, \quad (2.7)$$

where  $P$  is the average power.

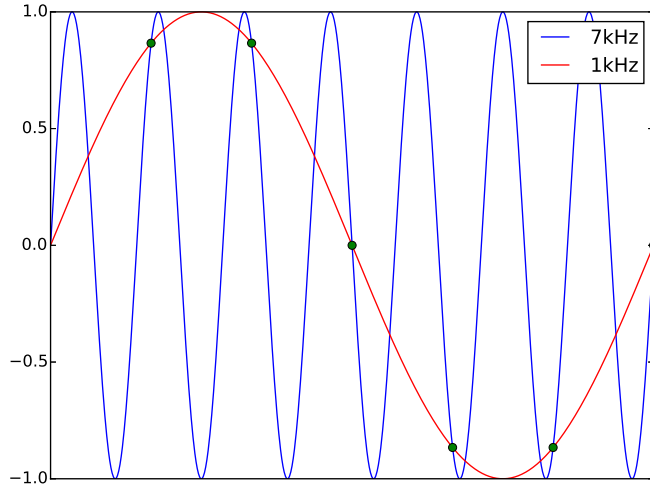


Figure 2.9: Example of signal ambiguity that happens if the sampling frequency is not the adequate, known as *aliasing*.

NMR technique is intrinsically poor in sensitivity; for that reason, several methods are usually employed to improve it such as electronic and digital filters in time and frequency domain.

Concerning dynamic range, it is defined as the range of signal intensities over which samples can be detected, equivalent to the ratio between the largest and lowest intensity. For example, in a spectrum the dynamic range is the ratio of the largest and smallest peak. The main difference between signal to noise ratio and dynamic range is that the former is an absolute limitation: it tells the minimum of signal height that can be distinguished regardless of any strong signals in the sample. However, the dynamic range is a relative limitation: it determines how small a signal can be detected in relation to the largest peak in the sample [26]. As shown in [15] NMR spectra usually has a large dynamic range because small and large peaks can happen together; for that reason, some problems -related to distinguish between signal and noise- arise in NMR.

### 2.2.2 Resolution

One more important aspect when recording NMR signal is obtaining a good resolution, understood as the capacity to obtain separated frequency bands from which the amplitude and position is not hidden by the overlapping. In Figure 2.12 a spectrum with low and great resolution is shown; it is obvious that when a spectrum has low resolution several different peaks will overlap together and consequently

only one peak would appear in the spectra and therefore some valuable information will be missing.

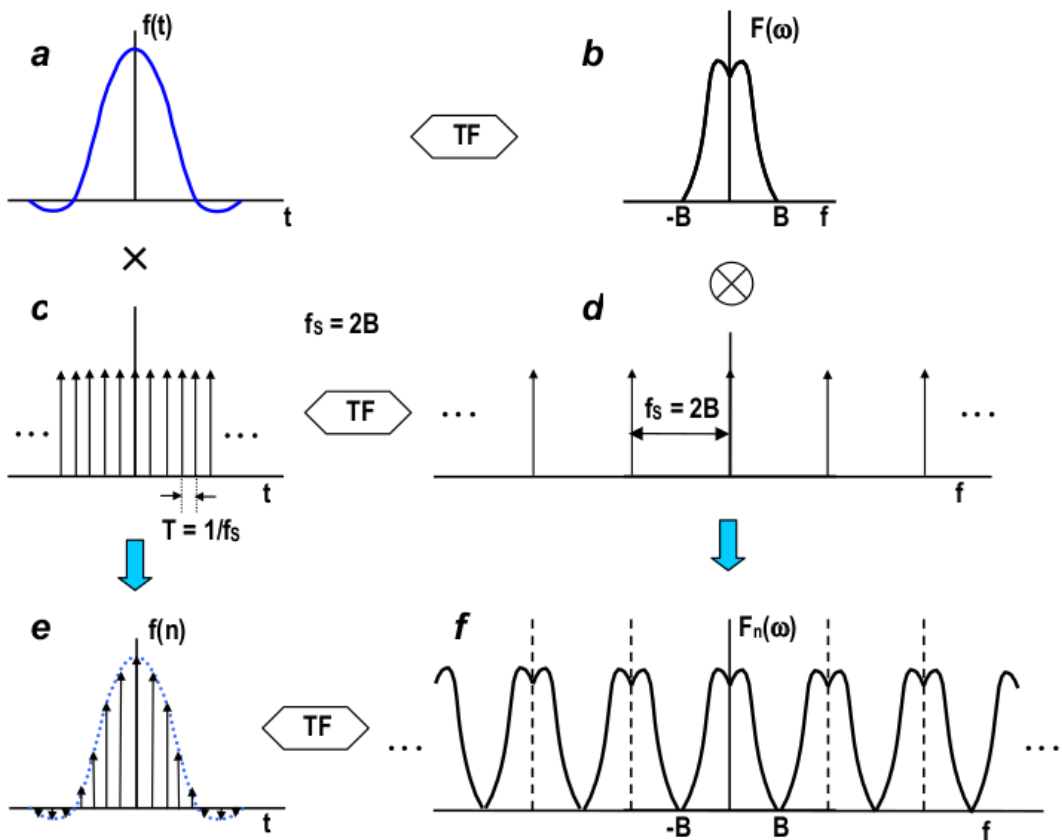


Figure 2.10: In picture *a* and *c* the original signal and a set of delta functions separated by  $1/f_s$  are shown respectively. Its Fourier transforms are shown in pictures *b* and *d*, it should be noted that now the set of Delta functions are separated by  $f_s$ . The discretized signal which is just the multiplication of *a* and *c* is plotted in picture *e*. Finally, the spectrum of the discretized signal which is equivalent to do the convolution of the spectrum of the original signal and the set of Delta functions is shown in picture *f*. As it can be seen, copies of the original spectrum occur, the reason is clear when considering the convolution of the original spectrum and the set of Delta functions. Image taken from [38].

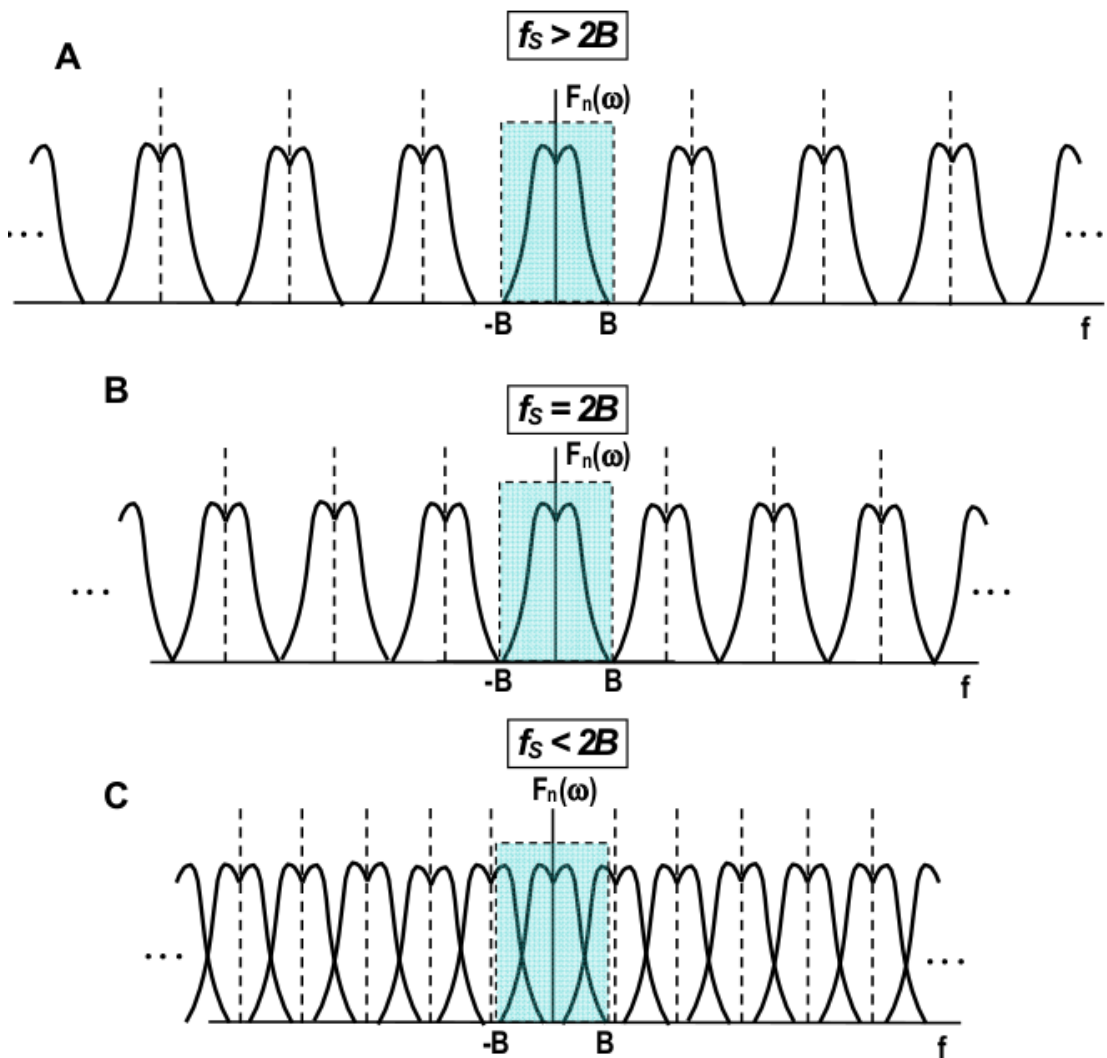


Figure 2.11: It is shown what happens by using different sampling frequencies. If  $f_s > 2B$  then copies of the spectrum are more separated between them, if  $f_s = 2B$  then there is no separation and if  $f_s < 2B$  then copies of the spectra overlap each other and aliasing occurs. Image taken from [38].

## 2.3 NMR Spectroscopy Signal Reconstruction Problem

In NMR spectroscopy, achieving a high resolution and sensitivity spectra by taking as few as possible number of samples is of primary importance. The sampling time is proportional to the number of sampled data points in the NMR signal; this

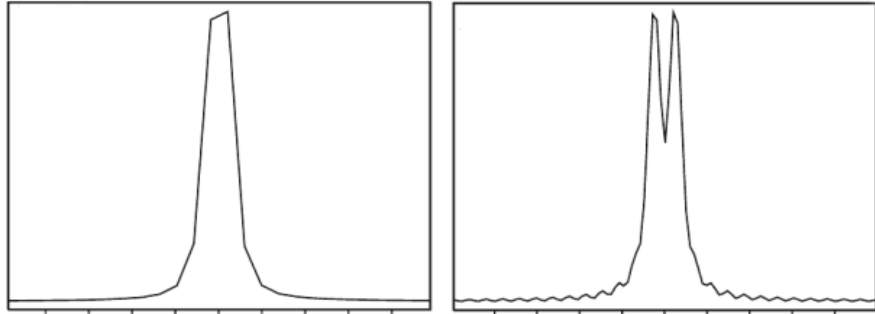


Figure 2.12: The left and right images are examples of a spectrum with low and high resolution respectively. As it can be seen, when a spectrum has low resolution then two near peaks will overlap and they will appear as just one big peak.

number increases with the resolution and dimensionality, mainly in the indirect time as demonstrated previously. As larger time implies higher costs, developing a method that acquires as few as possible data points and provides an accurate spectrum is one of the main goals. Sampling data points at not equally spaced random times, named in previous section as *non-uniform sampling* (NUS), offers the possibility of reducing dramatically the sampling time when applied to the indirect time. However, using NUS carries a drawback: if the signal is not uniformly sampled then it is not possible to obtain its spectrum by doing the Fourier transform; moreover further constraints or assumptions must be introduced in order to reconstruct the signal.

Several techniques have been recently developed to solve the problem by using different approaches. One of the possibilities is to pose the reconstruction as a deconvolution problem. Another approach consists in considering the problem as an optimization issue. In the next subsections both approaches will be described.

### 2.3.1 Reconstruction as a Deconvolution Problem

Doing Discrete Fourier transform (DFT) of non-uniformly sampled data (where zeros were inserted at not sampled points) is not theoretically correct because basis functions of the Fourier sum corresponding to missing data are eliminated. Therefore, basis functions interfere with each other and are no longer orthogonal. Nonetheless, the application of Fourier transform to non-uniformly sampled data could be useful by considering convolution theorem and posing the problem as a deconvolution problem.

Non-uniform sampling is equivalent to multiplying a signal by a vector of 0 and 1 values, where 0 represents not taken samples and 1 the taken ones. This vector is called the *schedule*. By using the convolution theorem, the result of applying DFT

to a non-uniformly sampled signal is equivalent to doing the convolution of the DFT of the signal with the DFT of the schedule, see Figure 2.13. The DFT of the schedule is a key aspect to understand the problem; the obtained spectra is called *point spread function* (PSF). The width of the main peak of the PSF determines how much the spectral features are broadened. Moreover, the amplitude of non-zero components of the PSF indicates the magnitude and position of the *artefacts*, i.e. peaks that are not present in the original spectra.

By taking into consideration all the previous informations, it can be seen that the problem can be stated as a deconvolution problem were the spectra of the schedule and the convolved spectra are known (in Figure 2.13 the two right images of the bottom row respectively). Although deconvolution can be done theoretically by dividing the DFT of the convolved signal with the PSF, several problems arise if the PSF has zero values (which is very common) or if the values are very low, which would imply results with large magnitudes and consequently small noise would be highly amplified. For that reason, other deconvolution techniques are used such as CLEAN algorithm that deconvolves signals iteratively [16].

### 2.3.2 Reconstruction as an Optimization Problem

As the data is not uniformly sampled and the number of samples does not fulfil the Nyquist criteria, then there is another kind of algorithms that try to reconstruct the signal by assuming some properties of the NMR signal. The correctness of these properties will determine the success of the method. In the following both compressed sensing and low-rank reconstruction method will be exposed. Moreover, a new method based on the previous ones will be proposed. As it is later shown, all these techniques assume different properties of the FID signal and impose them as constraints.

#### Compressed Sensing

The *compressed sensing* (CS) method is a popular technique that assumes that the NMR spectrum is sparse, in other words, that the spectrum only has a few high frequencies and the rest of the frequency domain is zero i.e. minimizes the zero norm of the spectrum.

CS problem can be stated as an optimization problem

$$\min_{\mathbf{s}} \|\mathbf{F}\mathbf{s} - \mathbf{y}\|_2^2 + \lambda \|\mathbf{s}\|_0, \quad (2.8)$$

where  $\mathbf{F} \in \mathbb{C}^{M \times N}$  is the inverse discrete Fourier transform matrix,  $\mathbf{s} \in \mathbb{C}^N$  is the spectrum and  $\mathbf{y} \in \mathbb{C}^M$  is the sampled data in the time domain where  $M$  is the number of taken samples using NUS so  $M < N$  being  $N$  the number of points of

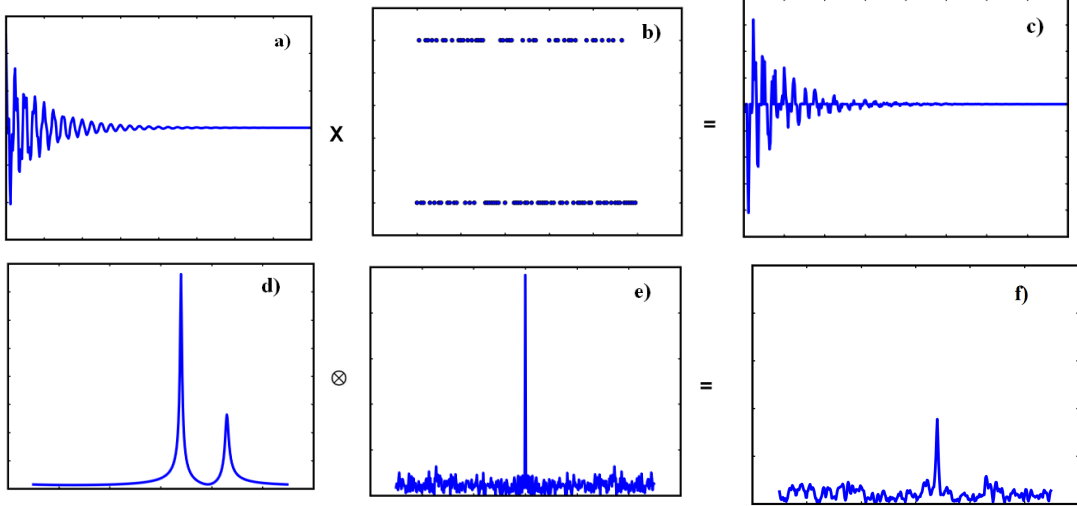


Figure 2.13: The top row shows data in the time domain and the bottom row shows the DFT of the top row data. The left column shows uniformly sampled signal and its DFT. In the central column a random sampling schedule can be seen (with 0's and 1's) and its DFT which is a *point spread function* (PSF) in the frequency domain. The right column shows the DFT of the signal non-uniformly sampled. The figure demonstrates that multiplying the time domain of a signal by a sampling schedule and doing its DFT is equivalent to do the convolution of the frequency domain spectrum with the point spread function, that is,  $DFT(a \times b) = DFT(c) = DFT(a) \otimes DFT(b) = d \otimes e = f$ . Note that the convolved signal intensity has decreased due to PSF maximum intensity is less than one.

the Fourier grid. Unfortunately, as  $l_0$  norm is not convex then minimizing it is a NP-hard problem and cannot be solved in a reasonable time. Fortunately, there is an alternative problem which consists on minimizing the  $l_1$  norm [43]

$$\min_{\mathbf{s}} \|\mathbf{Fs} - \mathbf{y}\|_2^2 + \lambda \|\mathbf{s}\|_1. \quad (2.9)$$

Problem (2.9) can be solved by converting the penalty function to an  $l_2$  norm by considering the fact that

$$\|\mathbf{s}\|_p^p = \sum_i w_i |s_i|^p \quad (2.10)$$

where  $w_i = |s_i|^{p-2}$ . This allows to formulate an equivalent problem to (2.9):

$$\min_{\mathbf{s}} \|\mathbf{Fs} - \mathbf{y}\|_2^2 + \|\mathbf{Ws}\|_2^2, \quad (2.11)$$

where  $\mathbf{W}$  is a diagonal matrix with elements  $W_{ii} = \sqrt{\lambda/|s_i|}$ . Considering  $\mathbf{e} = \mathbf{Fs} - \mathbf{y}$

then the solution to (2.11) is

$$\begin{aligned} \frac{\partial}{\partial s} [\mathbf{e}^T \mathbf{e} + (\mathbf{W}\mathbf{s})^T \mathbf{W}\mathbf{s}] &= -2\mathbf{F}^H \mathbf{y} + 2\mathbf{F}^H \mathbf{F}\mathbf{s} + 2\mathbf{W}^T \mathbf{W}\mathbf{s} = 0 \\ &= -\mathbf{F}^H \mathbf{y} + (\mathbf{F}^H \mathbf{F} + \mathbf{W}^2)\mathbf{s} = 0 \\ \implies \mathbf{s} &= (\mathbf{F}^H \mathbf{F} + \mathbf{W}^2)^{-1} \mathbf{F}^H \mathbf{y}. \end{aligned} \quad (2.12)$$

where  $\mathbf{F}^H$  is the conjugate transpose of  $\mathbf{F}$ .

As spectrum  $\mathbf{s}$  is unknown, then  $W_{ii}$  weights can not be determined exactly. For that reason, the right part of solution (2.12) must be solved iteratively by using the solution from previous iteration; that is, starting with  $\mathbf{W} = \mathbf{I}$  ( $\mathbf{I}$  being the identity matrix) and then update weights with the spectrum values of previous iteration. It should be noted that in order to avoid division by zero then a term  $\epsilon = 10^{-8}$  must be added to the denominator of the weight,  $W_{ii} = \sqrt{\lambda/(|s_i| + \epsilon)}$ , as explained in [10].

Although this technique has been quite popular, the sparseness of the NMR spectrum has been proved to be just a naïve approximation so in some situations the quality of the obtained spectrum does not fulfil the standards. For example, when the spectrum has broad peaks then the sparseness hypothesis fails and consequently the shape of the reconstructed spectrum gets distorted and even some peaks disappear.

### Low-Rank Reconstruction

Due to the drawbacks that appear in CS, alternative methods must be researched. In this project the *low-rank (LR) spectrum reconstruction* proposed in [42] is analyzed and implemented.

LR assumes that the time domain NMR signal can be approximated by a free induction decay signal

$$\text{FID} = \sum_{j=1}^J (A_j e^{i\phi_j}) e^{-t/\tau_j} e^{it\omega_j}, \quad (2.13)$$

where  $A_j$ ,  $\phi_j$ ,  $\tau_j$  and  $\omega_j$  are the amplitude, phase, decay time and angular frequency respectively. LR also assumes that the spectrum has the least number of spectral peaks, that is, the number of decaying exponentials,  $J$ , is assumed to be as small as possible (note the subtle difference with compressed sensing that seeks for a spectrum with the fewest non-zero spectral intensities). The rank of the FID signal is equal to the number of exponentials that is equivalent to the rank of  $\mathbf{X} = \mathbf{Rx}$  (see [8]), being  $\mathbf{R}$  the operator that converts a time domain signal vector

$\mathbf{x} \in \mathbb{C}^N$  to its Hankel matrix,

$$\mathbf{X} = \mathbf{R}\mathbf{x} = \begin{bmatrix} x(1) & x(2) & x(3) & \cdots & x(Q) \\ x(2) & x(3) & x(4) & \cdots & x(Q+1) \\ \vdots & \vdots & \vdots & \ddots & \vdots \\ x(N-Q) & x(N-Q+1) & x(N-Q+2) & \cdots & x(N-1) \\ x(N-Q+1) & x(N-Q+2) & x(N-Q+2) & \cdots & x(N) \end{bmatrix} \quad (2.14)$$

where  $\mathbf{X} \in \mathbb{C}^{(N-Q+1) \times Q}$  is a Hankel matrix,  $\mathbf{R} : \mathbb{R}^N \rightarrow \mathbb{R}^{(N-Q+1) \times Q}$  and  $Q$  is a parameter usually chosen as  $0.1N$ .

The core idea LR relies on is that a low-rank matrix can be recovered successfully just from a limited number of its elements [11]. This can be mathematically described as follows: LR reconstructs the spectrum by assuming that the FID signal can be approximated by a sum of few decaying sinusoidals, that is, sinusoidal signals with a time decaying term. Let  $\mathbf{x}$  be a vector with the complete FID signal and  $\mathbf{R}$  an operator that converts the vector into a Hankel matrix,  $\mathbf{X} = \mathbf{R}\mathbf{x}$ . If the FID signal has low rank, that means that the rank of the Hankel matrix is low, which can be equivalently stated as  $\mathbf{X}$  having a low number of singular values. When the FID signal is non-uniformly sampled then the matrix  $\mathbf{X}$  has missing values (remember that in NUS some values from Fourier grid are not taken). Thus, the idea is to get a NMR signal,  $\mathbf{x} \in \mathbb{C}^N$ , whose Hankel matrix rank is low, in optimization this can be stated as

$$\min_{\mathbf{x}} \|\mathbf{R}\mathbf{x}\|_* \quad (2.15)$$

where  $\|\cdot\|_*$  is the nuclear norm defined as the sum of the singular values of the matrix which determines quantitatively how low is the rank. In addition, it is also wanted that the  $\mathbf{x}$  signal matches as much as possible the experimentally recorded values, that is,

$$\|\mathbf{y} - \mathbf{U}\mathbf{x}\|_2^2 \quad (2.16)$$

should be as low as possible where  $\mathbf{y} \in \mathbb{C}^M$  is the non-uniformly sampled FID signal being  $N \geq M$  and  $\mathbf{U}$  is the NUS operator that selects random points from the Fourier grid (e.g. Poisson-gap). For that reason, the reconstruction problem can be stated as solving

$$\min_{\mathbf{x}} \|\mathbf{R}\mathbf{x}\|_* + \frac{\lambda}{2} \|\mathbf{y} - \mathbf{U}\mathbf{x}\|_2^2, \quad (2.17)$$

where  $\lambda$  is a parameter that regulates the low rank restriction and the consistency between the reconstructed signal  $\mathbf{x}$  and the experimental data  $\mathbf{y}$ .

The main advantage of LR with respect to CS is that the rank of the FID signal is independent on the line width, and therefore LR performs better reconstruction of line shapes for both sharp and broad peaks.

### Hybrid Method by Combining Compressed Sensing and Low-Rank Methods

In this master thesis an original novel reconstruction method is proposed. It is called *hybrid method* and is based on combining compressed sensing and low-rank methods.

The reconstruction method is posed as follows:

$$\min_{\mathbf{x}} \frac{\lambda}{2} \underbrace{\|\mathbf{y} - \mathbf{Ux}\|_2^2}_{(1)} + \underbrace{\|\mathbf{Rx}\|_*}_{(2)} + \underbrace{\|\mathbf{WFx}\|_2^2}_{(3)}, \quad (2.18)$$

where  $\mathbf{W}$  is a diagonal matrix with components  $W_{ii} = \sqrt{\alpha/|(\mathbf{F}\mathbf{x})_i|}$  being  $\alpha$  a trade-off parameter measuring the sparsity of the reconstructed signal and  $\mathbf{F}$  is the discrete Fourier transform matrix (do not confuse with the matrix used in compressed sensing that was the inverse). The term (1) represents consistency with measured data, term (2) is the Hankel low-rank regularity term and the last term adds the compressed sensing minimization norm.

This new method incorporates the low-rank and sparsity assumptions of both algorithms. With this approach it is intended to acquire the advantages of both algorithms at the same time.

## 2.4 Literature Survey

In this section current state-of-the-art will be discussed. Firstly, non-uniform sampling schedules will be shown and then several available reconstruction methods will be pointed out.

A key aspect of non-uniform sampling is to develop optimal sampling schedules. The first idea was given by Barna et al. who proposed to place the sampling points in the indirect dimension with exponentially decreasing separation and to obtain the spectra by using a maximum entropy algorithm [3]. After that, the main advantages of non-uniform sampling have been acknowledged by the scientific community in various occasions such as [45] and [21]. There were also some attempts to use uniform random sampling [40], [31] and hybrids between US and NUS. Nevertheless, it has been demonstrated [22] that Poisson-gap sampling is superior to previous sampling techniques.

After performing the sampling several algorithms must be used to recover the signal. Since Barna sampling and reconstruction method came up, other researchers have been trying to develop similar reconstruction methods by using again maximum entropy method implemented in various forms [20] or by developing CLEAN method for NMR signal reconstruction [14]. Also, Forward Maximum Entropy algorithm was developed [23] with good results.

Apart from maximum entropy methods other techniques have also been used recently such as the maximum likelihood method (MLM) [12], Fourier transformation for non-uniformly sampled data [37] and [29], multi-dimensional decomposition (MDD) [35] and [18], which assumes that a multidimensional spectrum can be modelled as a sum of components written as a direct product of 1D line shapes, Filter Diagonalization Method (FDM) which fits the time domain signal to sums of decaying sinusoidals, radial sampling [36] and GFT [33] and [13].

Moreover, as in non-uniform sampling the set of test functions in Fourier transform is no longer orthogonal then the set can be reduced in either time domain [28] or in the frequency domain [32] in order to make a fast conversion from the time domain to the frequency domain.

Finally, compressed sensing algorithm has been used for reconstruction by using different implementations based on the principle of iterative soft thresholding (IST) [24] which was demonstrated to be equivalent to the  $l_1$  norm reconstruction [44] or by using iterative re-weighted least square approach [30].

A more extensive review of used algorithms for FID signal reconstruction can be seen in [39].



# Chapter 3

## Methodology

The present chapter is divided into four sections. The first part consists on an extensive introduction to non-uniform sampling by using Poisson-gap method. In the second part several optimization techniques will be analyzed and solutions to the previously posed low-rank and hybrid optimization problems will be given. The next section will deal with the implementation of the optimization procedure. Finally, data that will be used in the experiments will be described.

### 3.1 Non-Uniform Sampling and Poisson-Gap

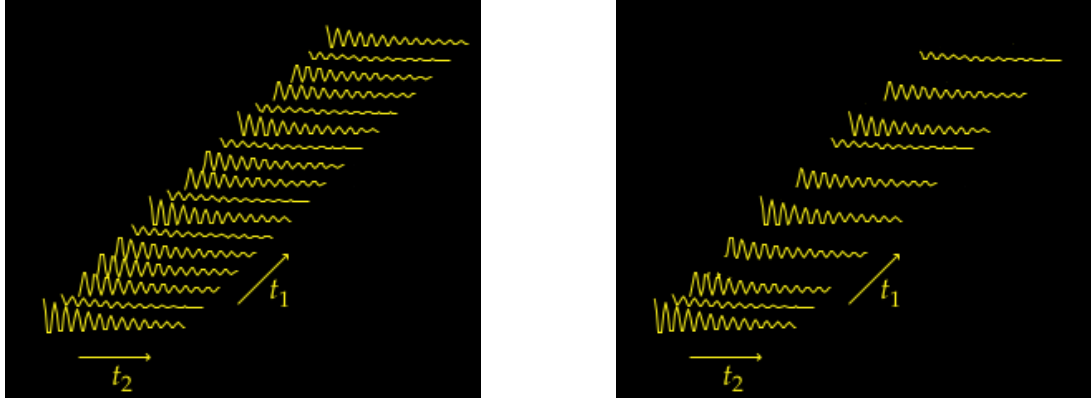
In the last thirty years much interest has been drawn to Non-Uniform Sampling (NUS), i.e. a technique in which samples are taken at not equally spaced time instants. When using NUS usually less samples than minimum are taken; therefore, according to Nyquist criterion the signal can not be recovered. However, the main idea when using NUS is to recover the original signal by using extra information related to the type of signal being sampled, which the experimenter should know about.

A good performance NUS method should fulfil the following characteristics [25]:

- (C1) large gaps in the sampling are not recommended,
- (C2) gaps at the beginning or end of the sampling are worse than in the middle.

As it was reviewed in the literature survey there are several NUS methods. In this work only Poisson-gap method will be used, as it has been proved to behave better than other sampling schedules [22]. The Poisson-gap sampling assigns a probability  $f$  for a specific gap size  $x \geq 0$  by following a Poisson distribution,

$$f(x, \lambda) = \frac{\lambda^x e^{-\lambda}}{x!}. \quad (3.1)$$



(a) Two-dimensional signal sampling when using US.

(b) Two-dimensional signal sampling when using NUS.

Figure 3.1: Example of applying US and NUS to a two-dimensional signal where  $t_1$  is the indirect dimension and  $t_2$  is the direct dimension. It should be noted that when using NUS less signals are sampled. Images taken from [19].

This probability satisfies requirement (C1). Moreover, (C2) is reached with the help of a sinusoidal variation of  $\lambda$ , that is,  $\lambda = \Lambda \sin \theta$  where  $\theta$  linearly spans from 0 to  $\pi/2$  and  $\Lambda$  controls the average of  $\lambda$ .

### 3.1.1 Advantages of Applying Non-Uniform Sampling to Multidimensional Spectrum

NUS is only useful when applied to multidimensional spectra. The reason is that when applied to a one-dimensional signal, only  $t_2$  (direct time) takes part and, as was explained in the previous chapter, no time gain is obtained. Nevertheless, if NUS is applied to a higher dimensional signal then some signals do not need to be sampled and therefore time is saved. For example, in the two-dimensional case, the direct dimension is always completely sampled but for the indirect dimension Poisson-gap is applied. See, for example, Figure 3.1 where a two dimensional signal is shown. If US is applied then all signals must be sampled but instead if NUS is used then it is not needed to sample all signals in the indirect dimension and time is saved.

## 3.2 Optimization Techniques

In this section, optimization techniques are analyzed in order to solve the problems presented in section 2.3.2. Its main goal is to explain the *alternating direction*

*method of multipliers* (ADMM) to solve the low-rank problem:

$$\min_{\mathbf{x}} \|\mathbf{Rx}\|_* + \frac{\lambda}{2} \|\mathbf{y} - \mathbf{Ux}\|_2^2. \quad (3.2)$$

ADMM is an evolution from several more naïve techniques. Therefore, for pedagogical and historical reasons, first simpler techniques will be explained in order to smoothly reach to the ADMM method.

### 3.2.1 Dual Ascent

Lets define a convex optimization problem with linear constraints,

$$\begin{aligned} & \min_{\mathbf{x}} && f(\mathbf{x}) \\ & \text{subject to} && \mathbf{Ax} = \mathbf{b} \end{aligned} \quad (3.3)$$

where  $\mathbf{A} \in \mathbb{R}^{M \times N}$ ,  $\mathbf{x} \in \mathbb{R}^N$ ,  $\mathbf{b} \in \mathbb{R}^M$  and  $f : \mathbb{R}^N \rightarrow \mathbb{R}$  is convex. The Lagrangian of the previous problem is defined as

$$L(\mathbf{x}, \lambda) = f(\mathbf{x}) + \lambda^T(\mathbf{Ax} - \mathbf{b}) \quad (3.4)$$

where  $\lambda$  is the Lagrange multiplier. Then, problem (3.3) is equivalent to

$$\min_{\mathbf{x}} \max_{\lambda} L(\mathbf{x}, \lambda) \equiv \min_{\mathbf{x}} \begin{cases} f(\mathbf{x}), & \text{if } \mathbf{Ax} = \mathbf{b} \\ \infty, & \text{if } \mathbf{Ax} \neq \mathbf{b} \end{cases} \quad (3.5)$$

and it is easy to see that this formulation forces  $\mathbf{x}$  to be in the feasible region,  $\mathbf{Ax} = \mathbf{b}$ . This problem is known as *primal problem*. Another problem arises if the min and max terms are flipped,

$$\max_{\lambda} \min_{\mathbf{x}} L(\mathbf{x}, \lambda) \quad (3.6)$$

which is known as the *dual problem* and  $g(\lambda) = \min_{\mathbf{x}} L(\mathbf{x}, \lambda)$  is the dual function. Lets define the solution for each problem as

$$\begin{aligned} \mathbf{x}^* &= \min_{\mathbf{x}} \max_{\lambda} L(\mathbf{x}, \lambda), \quad (\text{primal solution}) \\ \lambda^* &= \max_{\lambda} \min_{\mathbf{x}} L(\mathbf{x}, \lambda), \quad (\text{dual solution}), \end{aligned} \quad (3.7)$$

where  $\mathbf{x}^*$  and  $\lambda^*$  are the solutions to the primal and dual problems respectively. If strong duality holds, that is, if primal and dual solutions are equivalent, then:

$$\mathbf{x}^* = \min_{\mathbf{x}} L(\mathbf{x}, \lambda^*), \quad (3.8)$$

given there is only one minimizer of  $L(\mathbf{x}, \lambda)$ , for example if  $f$  is strictly convex.

The main idea behind dual ascent method is that when previous condition is fulfilled then both variables  $\mathbf{x}$  and  $\lambda$  can be solved alternatively. Dual ascent method solves the problem iteratively:

For time iteration  $k = 0, 1, \dots$

$$\mathbf{x}^{k+1} = \min_{\mathbf{x}} L(\mathbf{x}, \lambda^k) \quad (3.9)$$

$$\lambda^{k+1} = \lambda^k + \alpha^k (\mathbf{A}\mathbf{x}^{k+1} - \mathbf{b}). \quad (3.10)$$

where (3.9) is the  $\mathbf{x}$  minimization and (3.10) is the dual update,  $\alpha^k > 0$  being the step size. Two important points should be noted:

- (i) we cannot update the  $\lambda^{k+1}$  variable as

$$\lambda^{k+1} = \max_{\lambda} L(\mathbf{x}^{k+1}, \lambda) \quad (3.11)$$

because then it would take infinite values. For that reason,  $\lambda^{k+1}$  is updated using gradient ascent algorithm.

- (ii) if strong duality holds then  $\mathbf{x}^* = \min_{\mathbf{x}} L(\mathbf{x}, \lambda^*)$  where  $\lambda^*$  is the optimal dual so the step (3.9) converges to the optimal primal solution with the appropriate choice of  $\alpha^k$ .

The main advantage of this method is that if the objective function is separable,

$$f(\mathbf{x}) = f_1(x_1) + f_2(x_2) + \cdots + f_N(x_N) \quad (3.12)$$

then the optimization can be carried out in parallel so large problems can be solved faster (see Subsection 3.2.2). However, for non separable functions it often converges slower than more advanced methods.

### 3.2.2 Dual Decomposition

Assuming that  $f(\mathbf{x})$  is separable (3.12), where  $\mathbf{x} = (\mathbf{x}_1, \mathbf{x}_2, \dots, \mathbf{x}_I)$  and the variables  $\mathbf{x}_i \in \mathbb{R}^{n_i}$  are subvectors of  $\mathbf{x}$ , then Lagrangian function

$$\begin{aligned} L(\mathbf{x}, \lambda) &= \sum_{i=1}^I f_i(\mathbf{x}_i) + \lambda^T \left( \sum_{i=1}^I \mathbf{A}_i \mathbf{x}_i - \mathbf{b} \right) \\ &= \sum_{i=1}^I L_i(\mathbf{x}_i, \lambda) - \lambda^T \mathbf{b} \end{aligned} \quad (3.13)$$

where  $\mathbf{Ax} = \sum_{i=1}^I \mathbf{A}_i \mathbf{x}_i$  and  $L_i(\mathbf{x}_i, \lambda) = f_i(\mathbf{x}_i) + \lambda^T \mathbf{A}_i \mathbf{x}_i$ . Thus, the dual ascent algorithm can be written in the following way:

$$\mathbf{x}_i^{k+1} = \min_{\mathbf{x}_i} L_i(\mathbf{x}_i, \lambda^k), \quad i = 1, \dots, N \quad (3.14)$$

$$\lambda^{k+1} = \lambda^k + \alpha^k (\mathbf{Ax}^{k+1} - \mathbf{b}), \quad (3.15)$$

where each optimization problem of (3.14) can be handled by different processors in parallel.

### 3.2.3 Augmented Lagrangian and Methods of Multipliers

In the augmented Lagrangian method a strictly convex term is added to the Lagrangian to make the problem easier to solve and more robust. It also allows to yield convergence without some assumptions of dual ascent algorithm such as strict convexity of  $f$ . Thus, given a penalty parameter  $\rho > 0$ , the Lagrangian function has the form:

$$L_\rho(\mathbf{x}, \lambda) = f(\mathbf{x}) + \lambda^T (\mathbf{Ax} - \mathbf{b}) + \frac{\rho}{2} \|\mathbf{Ax} - \mathbf{b}\|_2^2. \quad (3.16)$$

As the additional term is equal to zero at any feasible point, then the optimal value does not change. In fact,

$$\begin{aligned} \underset{\mathbf{x}}{\text{minimize}} \quad & f(\mathbf{x}) \\ \text{subject to} \quad & \mathbf{Ax} = \mathbf{b} \end{aligned} \equiv \begin{aligned} \underset{\mathbf{x}}{\text{minimize}} \quad & f(\mathbf{x}) + \frac{\rho}{2} \|\mathbf{Ax} - \mathbf{b}\|_2^2 \\ \text{subject to} \quad & \mathbf{Ax} = \mathbf{b} \end{aligned} \quad (3.17)$$

because when  $\mathbf{Ax} = \mathbf{b}$  then  $\frac{\rho}{2} \|\mathbf{Ax} - \mathbf{b}\|_2^2 = 0$ .

By applying dual ascent method to (3.17) the solution can be found through the following algorithm:

For time  $k = 0, 1, \dots$

$$\begin{aligned} \mathbf{x}^{k+1} &= \min_{\mathbf{x}} L_\rho(\mathbf{x}, \lambda^k) \\ \lambda^{k+1} &= \lambda^k + \rho(\mathbf{Ax}^{k+1} - \mathbf{b}), \end{aligned} \quad (3.18)$$

which is known as the *method of multipliers*. In order to realize why  $\rho$  is used as step size parameter it should be recalled that for the primal problem (3.5)  $\mathbf{x}^*$  is optimum if

$$\nabla_{\mathbf{x}} L(\mathbf{x}, \lambda^*)|_{\mathbf{x}=\mathbf{x}^*} = 0 \implies \nabla f(\mathbf{x}^*) + \mathbf{A}^T \lambda^* = 0, \quad (3.19)$$

and, in the case of the augmented Lagrangian

$$\begin{aligned} \nabla_{\mathbf{x}} L_{\rho}(\mathbf{x}, \lambda^k) |_{\mathbf{x}=\mathbf{x}^{k+1}} &= 0 \\ \implies \nabla f(\mathbf{x}^{k+1}) + \mathbf{A}^T \lambda^k + \rho \mathbf{A}^T (\mathbf{A}\mathbf{x}^{k+1} - \mathbf{b}) &= 0 \\ \implies \nabla f(\mathbf{x}^{k+1}) + \mathbf{A}^T (\lambda^k + \rho(\mathbf{A}\mathbf{x}^{k+1} - \mathbf{b})) &= 0 \\ \text{if (3.18)} \implies \nabla f(\mathbf{x}^{k+1}) + \mathbf{A}^T \lambda^{k+1} &= 0 \end{aligned} \quad (3.20)$$

which is the optimal solution condition for the primal problem.

This method converges under more relaxed conditions, e.g.  $f$  does not need to be strictly convex. However, the main disadvantage is that the quadratic term inhibits the parallelization of the algorithm and therefore it shows a slower performance [6].

### 3.2.4 Alternating Direction Method of Multipliers

In order to overcome all the drawbacks that arise in the method of multipliers, the alternating direction method of multipliers (ADMM) was developed. Its purpose is to achieve the robustness of the method of multipliers while being as fast as dual descent [6]. The algorithm is based on the following idea: assuming that the objective function is separable  $f(x) = f_1(x_1) + f_2(x_2)$  (for simplicity  $N = 2$ ) and  $f_1$  and  $f_2$  are convex, then the augmented Lagrangian is

$$L_{\rho}(x_1, x_2, \lambda) = f_1(x_1) + f_2(x_2) + \lambda^T (A_1 x_1 + A_2 x_2 - b) + \frac{\rho}{2} \|A_1 x_1 + A_2 x_2 - b\|_2^2, \quad (3.21)$$

and ADMM solves each direction alternatively

$$x_1^{k+1} = \min_x L_{\rho}(x_1, x_2^k, \lambda^k) \quad (3.22)$$

$$x_2^{k+1} = \min_x L_{\rho}(x_1^{k+1}, x_2, \lambda^k) \quad (3.23)$$

$$\lambda^{k+1} = \lambda^k + \rho(A_1 x_1^{k+1} + A_2 x_2^{k+1} - b). \quad (3.24)$$

This algorithm is still not parallelizable because steps (3.22) and (3.23) are solved sequentially; however as step (3.23) uses  $x_1^{k+1}$  instead of  $x_1^k$  then the algorithm converges faster than the method of multipliers. It is true that (3.22) and (3.23) could be solved simultaneously (using  $x_1^k$  instead of  $x_1^{k+1}$  in equation (3.23)) but in that case the convergence would be much slower and the results could be different [5].

As indicated in [6] ADMM can be very slow to convergence to high accuracy. Nevertheless, it can be obtained a good accuracy for practical purposes just in a few tens of iterations. This quality makes the algorithm a good choice for this project because it offers a good trade-off between time and accuracy that is assumable by the industry.

### 3.2.5 Application of ADMM to the Reconstruction Problem Using Low-Rank Method

In order to solve the original optimization problem

$$\min_{\mathbf{x}} \|\mathbf{Rx}\|_* + \frac{\lambda}{2} \|\mathbf{y} - \mathbf{Ux}\|_2^2, \quad (3.25)$$

a similar approach to [46] will be used. The key point is that by using this approach the original problem can be simplified to an iterative algorithm where each step will have a closed form solution. Following this approach equation (3.25) is restated as

$$\begin{aligned} \min_{\mathbf{x}, \mathbf{Z}} \quad & \|\mathbf{Z}\|_* + \frac{\lambda}{2} \|\mathbf{y} - \mathbf{Ux}\|_2^2 \\ \text{subject to} \quad & \mathbf{Rx} = \mathbf{Z} \end{aligned} \quad (3.26)$$

then the Lagrangian is

$$\Lambda(\mathbf{x}, \mathbf{Z}) = \|\mathbf{Z}\|_* + \frac{\lambda}{2} \|\mathbf{y} - \mathbf{Ux}\|_2^2 + \langle \mathbf{D}, \mathbf{Rx} - \mathbf{Z} \rangle. \quad (3.27)$$

where  $\mathbf{D}$  is the Lagrange multiplier and  $\langle \cdot, \cdot \rangle$  is the inner product of matrices defined as  $\langle \mathbf{A}, \mathbf{B} \rangle = \mathbb{R}\langle \mathbf{A}(:, \mathbf{B}(:, \cdot)) \rangle = \mathbb{R}(\text{trace}(\mathbf{A}^* \mathbf{B}))$  where  $\mathbb{R}(\cdot)$  denotes the real part. Thus, an equivalent problem to the original one can be constructed using the Lagrangian

$$\max_{\mathbf{D}} \min_{\mathbf{x}, \mathbf{Z}} \Lambda(\mathbf{x}, \mathbf{Z}). \quad (3.28)$$

By using the augmented Lagrangian

$$\max_{\mathbf{D}} \min_{\mathbf{x}, \mathbf{Z}} \Lambda(\mathbf{x}, \mathbf{Z}) + \frac{\beta}{2} \|\mathbf{Rx} - \mathbf{Z}\|_F^2 \quad (3.29)$$

and this dual problem can be solved by ADMM method since all terms are convex. In this case the alternating direction minimization would be:

$$\left\{ \begin{array}{l} \mathbf{x}^{k+1} = \min_{\mathbf{x}} \frac{\lambda}{2} \|\mathbf{y} - \mathbf{Ux}\|_2^2 + \langle \mathbf{D}^k, \mathbf{Rx}^k - \mathbf{Z}^k \rangle + \frac{\beta}{2} \|\mathbf{Rx}^k - \mathbf{Z}^k\|_F^2 \\ \mathbf{Z}^{k+1} = \min_{\mathbf{Z}} \|\mathbf{Z}\|_* + \langle \mathbf{D}^k, \mathbf{Rx}^{k+1} - \mathbf{Z}^k \rangle + \frac{\beta}{2} \|\mathbf{Rx}^{k+1} - \mathbf{Z}^k\|_F^2 \\ \mathbf{D}^{k+1} = \mathbf{D}^k + \tau (\mathbf{Rx}^{k+1} - \mathbf{Z}^{k+1}) \end{array} \right. \quad (3.30)$$

where  $\tau$  is the step size and for  $\tau = \beta = 1$  the algorithm converges [42]. Hereinafter,  $k$  superscript will be omitted for the sake of simplicity although it must be considered.

First equation of (3.30) is equivalent (same minimizer) to

$$\min_{\mathbf{x}} \frac{\lambda}{2} \|\mathbf{y} - \mathbf{U}\mathbf{x}\|_2^2 + \frac{\beta}{2} \|\mathbf{Rx} - \mathbf{Z} + \frac{\mathbf{D}}{\beta}\|_F^2, \quad (3.31)$$

which has closed-form solution. It can be calculated by

$$\begin{aligned} 0 &= \nabla_{\mathbf{x}} \left( \frac{\lambda}{2} \|\mathbf{y} - \mathbf{U}\mathbf{x}\|_2^2 + \frac{\beta}{2} \|\mathbf{Rx} - \mathbf{Z} + \frac{\mathbf{D}}{\beta}\|_F^2 \right) \\ &= \lambda (\mathbf{U}^T(\mathbf{U}\mathbf{x} - \mathbf{y})) + \beta \left( \mathbf{R}^T \left( \mathbf{Rx} - \mathbf{Z} + \frac{\mathbf{D}}{\beta} \right) \right) \\ &= \lambda (\mathbf{U}^T \mathbf{U} \mathbf{x} - \mathbf{U}^T \mathbf{y}) + \beta \left( \mathbf{R}^T \mathbf{R} \mathbf{x} - \mathbf{R}^T \mathbf{Z} + \mathbf{R}^T \frac{\mathbf{D}}{\beta} \right) \Rightarrow \\ \beta \mathbf{R}^T \mathbf{R} \mathbf{x} + \lambda \mathbf{U}^T \mathbf{U} \mathbf{x} &= \lambda \mathbf{U}^T \mathbf{y} + \beta \mathbf{R}^T \left( \mathbf{Z} - \frac{\mathbf{D}}{\beta} \right) \Rightarrow \\ \mathbf{x} &= (\beta \mathbf{R}^T \mathbf{R} + \lambda \mathbf{U}^T \mathbf{U})^{-1} \left( \lambda \mathbf{U}^T \mathbf{y} + \beta \mathbf{R}^T \left( \mathbf{Z} - \frac{\mathbf{D}}{\beta} \right) \right). \end{aligned} \quad (3.32)$$

Second equation of (3.30) is equivalent to the singular value shrinkage operator defined in [7], which as stated in Theorem 2.1 of the same reference it has a closed-form solution defined as

$$\mathbf{Z} = S_{1/\beta} \left( \mathbf{Rx} + \frac{\mathbf{D}}{\beta} \right) \quad (3.33)$$

where  $S_\eta$  is the soft singular value thresholding operator defined by  $S_\eta(\mathbf{X}) = \mathbf{U}S_\eta(\Sigma)\mathbf{V}^*$ ,  $S_\eta(\Sigma) = \text{diag}(\{\sigma_i - \eta\}_+)$ , where  $t_+ = \max(0, t)$  and  $\mathbf{U}\Sigma\mathbf{V}^*$  is the singular value decomposition (SVD) of matrix  $\mathbf{X}$ .

### 3.2.6 Application of ADMM to the Reconstruction Problem Using Hybrid Method

The optimization problem posed by the hybrid method can be solved by using similar techniques as low-rank. Thus, the equivalent augmented Lagrangian problem is:

$$\max_{\mathbf{D}} \min_{\mathbf{x}, \mathbf{Z}} \|\mathbf{Z}\|_* + \frac{\lambda}{2} \|\mathbf{y} - \mathbf{U}\mathbf{x}\|_2^2 + \|\mathbf{W}\mathbf{F}\mathbf{x}\|_2^2 + \langle \mathbf{D}, \mathbf{Rx} - \mathbf{Z} \rangle + \frac{\beta}{2} \|\mathbf{Rx} - \mathbf{Z}\|_F^2, \quad (3.34)$$

and using ADMM this can be solved as:

$$\begin{cases} \mathbf{x}^{k+1} = \min_{\mathbf{x}} \frac{\lambda}{2} \|\mathbf{y} - \mathbf{U}\mathbf{x}^k\|_2^2 + \|\mathbf{W}\mathbf{F}\mathbf{x}^k\|_2^2 + \langle \mathbf{D}^k, \mathbf{R}\mathbf{x}^k - \mathbf{Z}^k \rangle + \frac{\beta}{2} \|\mathbf{R}\mathbf{x}^k - \mathbf{Z}^k\|_F^2 \\ \mathbf{Z}^{k+1} = \min_{\mathbf{Z}} \|\mathbf{Z}^k\|_* + \langle \mathbf{D}^k, \mathbf{R}\mathbf{x}^{k+1} - \mathbf{Z}^k \rangle + \frac{\beta}{2} \|\mathbf{R}\mathbf{x}^{k+1} - \mathbf{Z}^k\|_F^2 \\ \mathbf{D}^{k+1} = \mathbf{D}^k + \tau (\mathbf{R}\mathbf{x}^{k+1} - \mathbf{Z}^{k+1}) \end{cases} \quad (3.35)$$

It can be observed that the last two equations are identical to the ones obtained by low-rank method. However, the first one has one more term,  $\|\mathbf{W}\mathbf{F}\mathbf{x}^k\|_2^2$ , which makes more difficult its resolution. Then, the solution to the first step is

$$\mathbf{x} = (\beta \mathbf{R}^T \mathbf{R} + \lambda \mathbf{U}^T \mathbf{U} + 2 \mathbf{F}^H \mathbf{W}^2 \mathbf{F})^{-1} \left( \lambda \mathbf{U}^T \mathbf{y} + \beta \mathbf{R}^T \left( \mathbf{Z} - \frac{\mathbf{D}}{\beta} \right) \right). \quad (3.36)$$

As the matrix  $\mathbf{W}$  is unknown this equation must be solved iteratively as done when solving compressed sensing problem. This carries the drawback that the hybrid algorithm is going to be much slower than low-rank algorithm. It must be taken into account that ADMM method is iterative and therefore in order to be feasible to use it the solutions to the subproblems must be closed (as in the case of low-rank method). However, in the case of the hybrid method the solution to  $\mathbf{x}^{k+1}$  is not closed (we have  $\mathbf{W}$  in the equation) and it must be solved iteratively which will take more time than low-rank algorithm.

### 3.3 Algorithms Implementation

For the implementation, Python programming language was used with the support of Numpy and Scipy scientific programming libraries. In the following it will be discussed how to implement the critical parts of the project.

Regarding the Poisson-Gap method it is important to develop a fast way of sampling a Poisson distribution. The great computer scientist Donald Knuth proposed the following pseudocode in [34] where a value of  $\lambda$  is received as input and the function returns an  $x$  that follows a Poisson distribution.

```
int poisson(double lmbd)
{
    double L = exp(-lmbd);
    int k = 0;
    double p = 1;

    do{
        double u=rand48();
        if(u<=L)
            k++;
        else
            break;
        L = L*(lmbd/k);
    }while(k<=lmbd);
    return k;
}
```

```

    p *= u;
    k += 1;
}while(p>=L);

return(k-1)
}

```

Concerning the ADMM algorithm, the bottleneck is the soft singular value threshold operator defined in (3.33). This handicap can be overcome by computing the singular value thresholding (SVT) without SVD, as shown in [9]. According to the authors of the previous reference, in the case where the rank of the matrix is not low compared to the matrix dimensions (note that it is the case of equation (3.33) because  $\mathbf{R}\mathbf{x} + \mathbf{D}/\beta$  does not have low rank) their method is much faster than computing the SVT with SVD. Their method to solve the SVT problem

$$D_\tau(\mathbf{Y}) = \min_{\mathbf{X}} \frac{1}{2} \|\mathbf{Y} - \mathbf{X}\|_F^2 + \tau \|\mathbf{X}\|_* \quad (3.37)$$

can be summarised as follows:

1. Compute the polar decomposition  $\mathbf{Y} = \mathbf{W}\mathbf{Z}$  without using singular value decomposition where  $\mathbf{W}$  is a unitary matrix and  $\mathbf{Z}$  is a positive-semidefinite Hermitian matrix.
2. Compute  $P_\tau(\mathbf{Z}) = \min_{\|\mathbf{X}\|_2 \leq \tau} \|\mathbf{X} - \mathbf{Z}\|_F$  via matrix iteration.
3. The solution to the problem is  $D_\tau(\mathbf{Y}) = \mathbf{Y} - \mathbf{W}P_\tau(\mathbf{Z})$ .

The authors state that their algorithm saves more than 50 per cent CPU time from the algorithm via the full SVD.

Nevertheless, a test was done by implementing this algorithm using Python programming language. Time comparisons were done between SVT implemented with their algorithm and also with SVD. For some reason, the time savings that they present were not achieved in practice. In fact, the time spent by this algorithm was twice compared to the SVT implemented by SVD.

## 3.4 Datasets

The algorithms were tested with two different types of signal datasets: a synthetic dataset and the dataset provided by Mestrelab Research based on experimental data obtained in a laboratory.

The synthetic dataset was created by generating free induction decay signals and adding some Gaussian noise in order to simulate experimental errors.

Regarding experimental data, a two dimensional spectra is shown in Figure 3.2 where experimental signals were taken from. This image shows an heteronuclear single quantum coherence (HSQC) NMR bidimensional spectrum; the spectrum corresponds to the discrete Fourier transform of 96 experimental FIDs measured in the direct dimension. A total of fifteen traces were taken in F2 (measured in parts per million): 2.187, 2.406, 2.539, 2.954, 3.103, 5.608, 5.914, 6.438, 6.689, 6.963, 7.746, 8.255, 8.748, 8.505 and 8.999. First ten traces correspond to signals and last five are noise. Each trace has 96 complex values equally spaced in F1; therefore its sampling frequency is 96. In Figure 3.3 the DFT of the fifteen traces are shown; it is clear that the last five are pure noise and for that reason they will not be used in the experiments. Further analysis of this data will be given in Section 4.2.

The reader may remark that the used traces shown in Figure 3.3 are one-dimensional and therefore no time gain is obtained when using non-uniform sampling (remember that higher resolution in  $t_2$  takes no more time). That is completely true and in fact applying non-uniform sampling is only useful for two-dimensional or higher dimension spectra (see Subsection 3.1.1). However, Mestrelab suggested to apply the low-rank algorithm to one-dimensional signals because if accuracy and resolution tests were successful then these results could be applied trivially to higher dimensions.

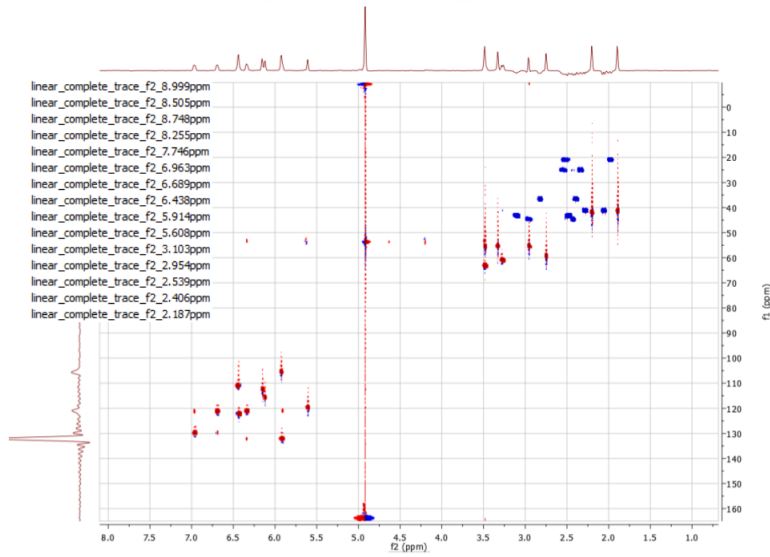


Figure 3.2: HSQC NMR bidimensional spectrum from where experimental signals were taken from.

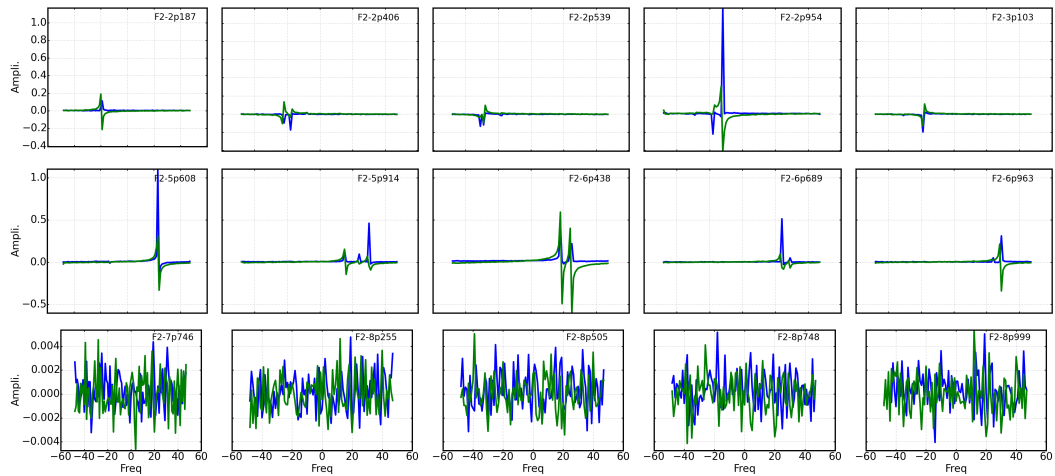


Figure 3.3: DFT of the experimental signals that were used in the analysis; blue and green lines correspond to real and imaginary parts of the spectrum respectively. It can be seen that last five signals are just noise.

# Chapter 4

## Results and Discussion

In the first section of this chapter compressed sensing, low-rank and hybrid algorithms are compared in terms of accuracy and computational time. In the next section, the effect of low-rank algorithm parameters on the accuracy of obtained spectra is described. Then, some results on the changes in peak areas of reconstructed spectra are provided. Moreover, some experiments are performed about the resolution quality of obtained spectra by using low-rank. Finally, brief notes are given about the randomness of obtained results produced by Poisson-gap sampling scheme.

### 4.1 Comparison between Low-Rank, Compressed Sensing and Hybrid Algorithms

In this section low-rank, compressed sensing and hybrid algorithms are going to be compared. The analysis consists on comparing reconstructed spectra by using the experimental data provided by Mestrelab. The comparisons are done in terms of spectrum accuracy and computing time.

#### 4.1.1 Spectra Accuracy Comparison

Table 4.1 shows the mean relative  $L^2$  error of reconstructed spectra and its standard error over 100 simulations for the three algorithms using a NUS ratio of 0.4 (ratio between sampled points and total points of US). In each simulation the signal was sampled with a random Poisson-gap NUS sampling schedule.  $L^2$  relative error is defined as:

$$\frac{\|S_{US} - S_{NUS}\|_2}{\|S_{US}\|_2} \quad (4.1)$$

<b>Signal</b>	<b>LR</b>	<b>CS</b>	<b>Hybrid</b>
F2-2.187	$0.0756 \pm 0.9 \times 10^{-3}$	$0.2462 \pm 6.4 \times 10^{-3}$	$0.0913 \pm 1.4 \times 10^{-3}$
F2-2.406	$0.2644 \pm 1.2 \times 10^{-2}$	$0.2668 \pm 0.4 \times 10^{-2}$	$0.2064 \pm 4.8 \times 10^{-3}$
F2-2.539	$0.3298 \pm 9.6 \times 10^{-3}$	$0.2715 \pm 3.7 \times 10^{-3}$	$0.2331 \pm 4.5 \times 10^{-3}$
F2-2.954	$0.0758 \pm 3.4 \times 10^{-3}$	$0.1139 \pm 0.3 \times 10^{-2}$	$0.0705 \pm 1.8 \times 10^{-3}$
F2-3.103	$0.1072 \pm 1.5 \times 10^{-3}$	$0.2271 \pm 0.4 \times 10^{-2}$	$0.1151 \pm 1.5 \times 10^{-3}$
F2-5.608	$0.0379 \pm 0.8 \times 10^{-3}$	$0.1393 \pm 0.6 \times 10^{-2}$	$0.0479 \pm 0.1 \times 10^{-2}$
F2-5.914	$0.1840 \pm 5.7 \times 10^{-3}$	$0.2413 \pm 5.5 \times 10^{-3}$	$0.1737 \pm 0.4 \times 10^{-2}$
F2-6.438	$0.0654 \pm 0.4 \times 10^{-2}$	$0.2927 \pm 1.0 \times 10^{-2}$	$0.1474 \pm 0.5 \times 10^{-2}$
F2-6.689	$0.0890 \pm 3.2 \times 10^{-3}$	$0.1577 \pm 2.7 \times 10^{-3}$	$0.0885 \pm 1.8 \times 10^{-3}$
F2-6.963	$0.0805 \pm 0.2 \times 10^{-2}$	$0.2047 \pm 5.9 \times 10^{-3}$	$0.0977 \pm 1.6 \times 10^{-3}$
<b>Average</b>	<b>0.1310</b>	<b>0.2161</b>	<b>0.1272</b>

Table 4.1: Mean  $L^2$  relative error (and its standard error) of reconstructed spectra using LR, CS and hybrid methods with a NUS ratio of 0.4 over 100 simulations.

where  $\|\cdot\|_2$  is the Euclidean norm,  $S_{US}$  is the spectrum obtained from uniform sampling (usually just performing the Fourier Transform) and  $S_{NUS}$  is the reconstructed spectrum from non-uniform sampling.

By comparing the results it is evident that low-rank and hybrid algorithms reconstruct more accurate spectra than the compressed sensing algorithm. Only for signals F2-2.406 and F2-2.539 the relative error is similar for all methods although a possible explanation is that signals have a high content of noise (see Section 4.2) and therefore the reconstruction is not good enough even when using a NUS ratio of 0.4.

### 4.1.2 Computing Time Comparison

The average time to reconstruct a signal of 96 points was 0.53, 1.46, and 2.19 seconds for low-rank, compressed sensing and hybrid algorithm, respectively. The calculations were performed on a laptop computer with an Intel Core i7 processor and 8 GB RAM. It should also be remarked that the low-rank algorithm does not always converge -in particular for the F2-6.438 signal- although the reconstructed spectra is always accurate.

### 4.1.3 Brief Discussion about the Algorithms

From the previous experiment, it can be seen that, in terms of reconstructed spectra accuracy, low-rank and hybrid algorithms perform far better than compressed

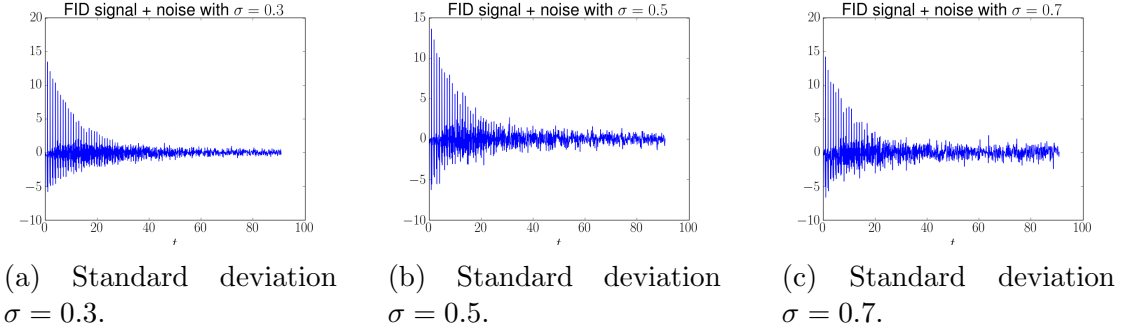


Figure 4.1: Synthetic signals used for the experiments with different Gaussian noise.

sensing algorithm. Moreover, if the calculation time is taken into account then low-rank is the fastest algorithm. For these reasons, and also because of the interest of Mestrelab company in the low-rank algorithm, a deep analysis is going to be done about the performance of low-rank algorithm and the others are going to be discarded although further analysis in the hybrid method should be done in the future because it is evident that outperforms low-rank algorithm in the reconstruction of some signals. Thus, hereinafter, all the reconstructed spectra and experiments will be performed by the low-rank algorithm.

## 4.2 Low-Rank Algorithm Parameters and Their Effects On the Accuracy of the Reconstructed Spectrum

The idea of the next experiment is to determine how low-rank parameters,  $\lambda$  and NUS ratio, affect the accuracy of the reconstructed spectrum. Both synthetic and experimental data were used. In Figure 4.1 the three used synthetic signals are shown. Results for these signals are shown in Figures 4.2 and 4.3. Results for experimental data are shown in Figures 4.4 and Figure 4.5. Moreover, the reconstructed spectra of experimental samples are shown in Figures 4.6 and 4.7, as it was divided in two parts for space purposes.

The first conclusion that can be derived is that  $\lambda$  parameter does not affect significantly on the reconstruction of a spectrum as far as  $\lambda \geq 10$ . Larger errors are obtained for  $5 \leq \lambda \leq 10$ .

In the case of NUS ratio, larger ratios imply lower errors, as expected. It can be seen that results are in general very accurate when using a NUS ratio  $\geq 0.2$ . However, we can also observe that in the case of experimental signals the

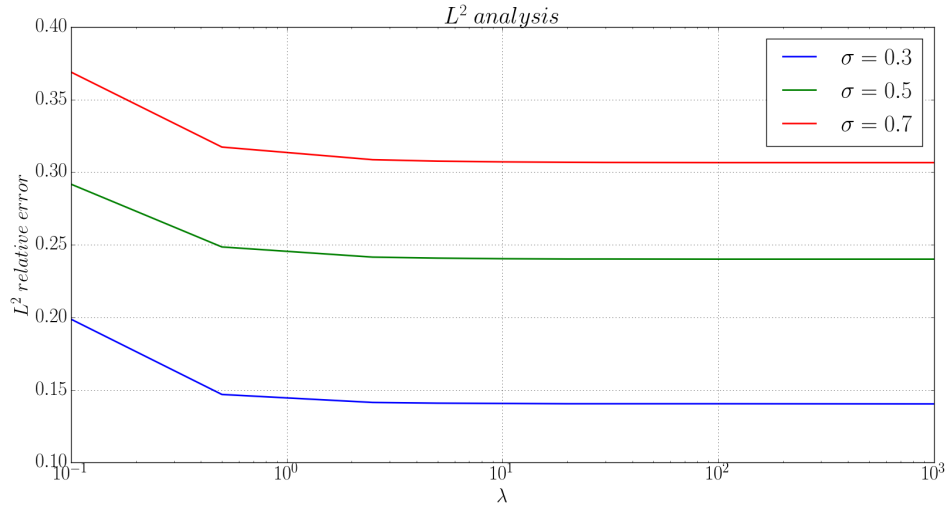


Figure 4.2:  $L^2$  relative error for synthetic data with a fixed NUS ratio of 0.2 by using different  $\lambda$  and Gaussian noise standard deviation values.

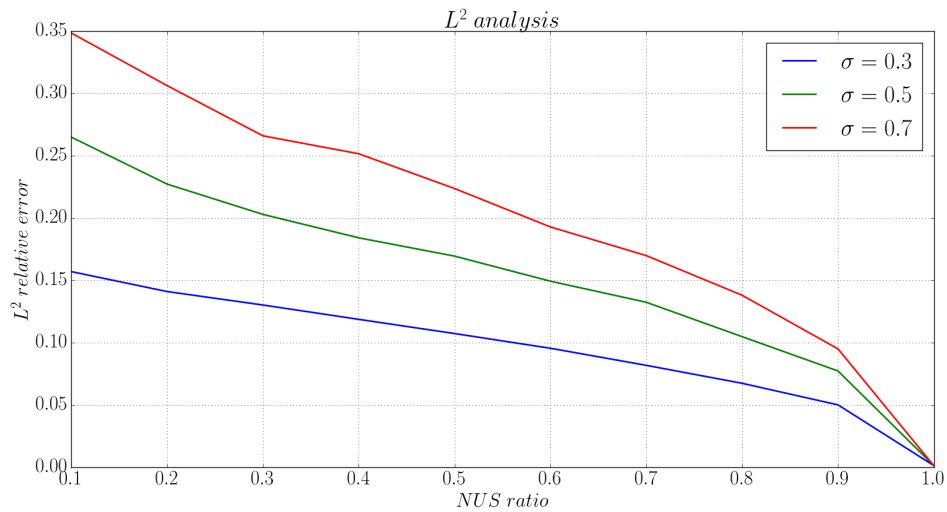


Figure 4.3:  $L^2$  relative error for synthetic data with  $\lambda = 10$  by using different NUS ratio and Gaussian noise standard deviation values.

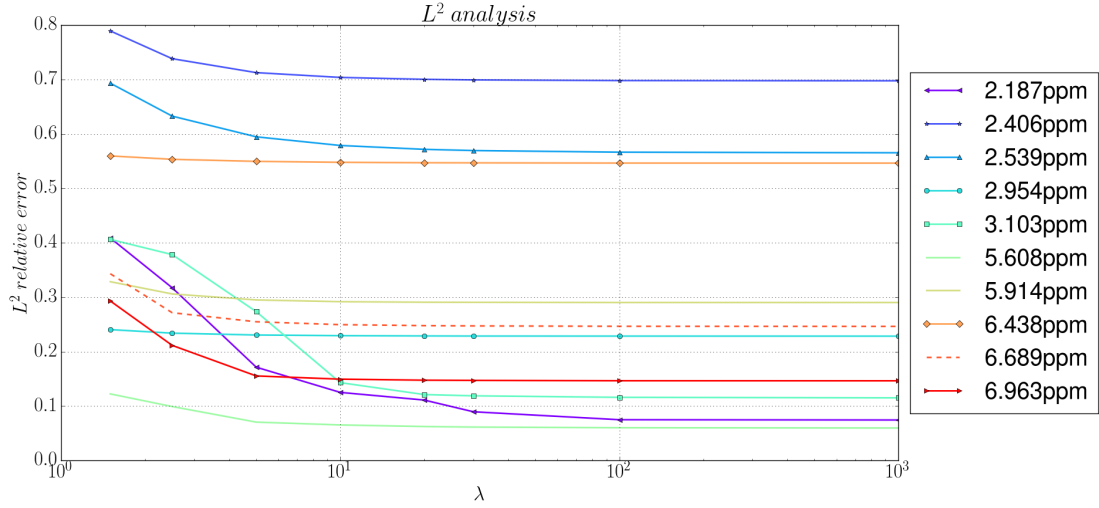


Figure 4.4:  $L^2$  relative error for experimental data by using different  $\lambda$  values and a fixed NUS ratio of 0.2.

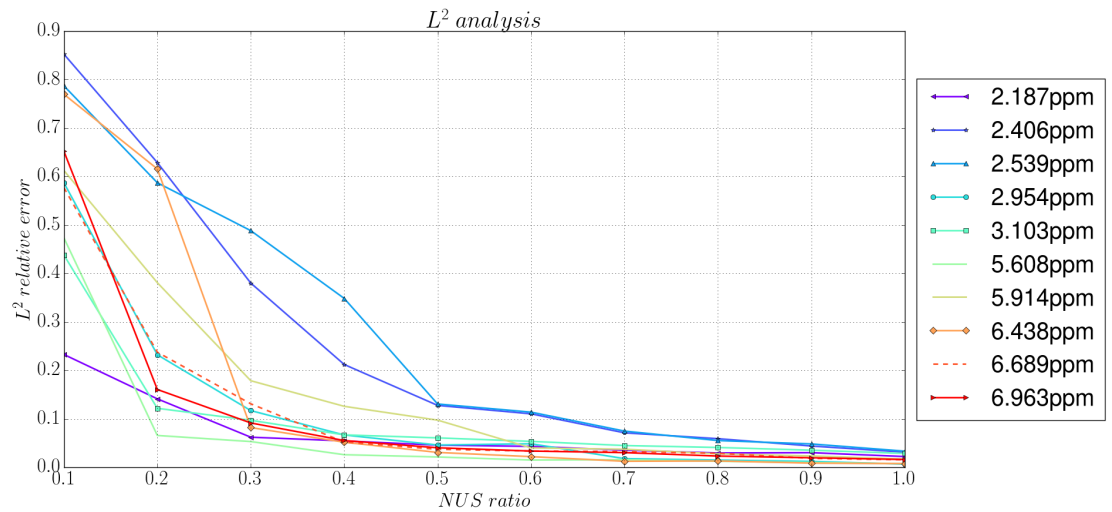


Figure 4.5:  $L^2$  error for experimental data by using different NUS values and  $\lambda = 10$ .

reconstructions for F2-2.406, F2-2.539, F2-5.914 and F2-6.438 signals are quite inaccurate using a ratio of 0.2. The reason can be explained by taking into account the noise appearing in the 2D spectrum shown in Figure 4.8. This image shows two intensity thresholds of the 2D spectra where experimental signals were taken from. Dots show coordinates where the amplitude of the spectrum is equal to a given value; red dots are related to positive noise values whereas blue dots correspond to negative noise. In this case, the intensity of the spectrum is really low to show the existence of noise in different parts of the spectrum and its tendency to gather in bands along some fixed  $f_2$  coordinates, e.g. blue bands at  $f_2 \approx 2.5$  and red bands at  $f_2 \approx 5.5 - 7.0$ . For some experimental reasons, red dots are related to better results of the two DFTs while blue dots correspond to worse defined results, that is, blue points have a greater noise intensity than red points. For that reason, reconstructions of signals F2-2.406, F2-2.539, F2-5.914 and F2-6.438, located at 2.406, 2.539, 5.914 and 6.438 ppm  $f_2$  frequency bands respectively, are inaccurate. In that frequency bands the effective noise is much bigger because there is a high density of blue points. To sum up, signals near the frequency bands where the density of blue points is high are much more difficult to reconstruct because of their high noise content. That is the reason why F2-2.406, F2-2.539, F2-5.914 and F2-6.438 signals are more difficult to reconstruct and a bigger NUS ratio is needed for that signals. In general, it can be concluded that a NUS ratio of 0.2 performs fine for signals with few noise and a NUS ratio greater or equal to 0.4 would obtain really accurate results for most signals even with high noise levels.

### 4.3 Differences in Peaks Area between Original and Low-Rank Reconstructed Spectrum

An important feature of a spectrum is the measure of the area under a peak, because it is proportional to the number of nuclei in a given chemical environment in a molecule. Obviously, this data provides important information for the scientists. For that reason, an experiment that measures peaks area differences between original and reconstructed spectrum was performed. It consisted on three steps:

1. Reconstruction of the signal from non-uniformly taken samples.
2. Decomposition of the domain of the spectrum in small regions around the peaks.
3. Measuring the relative error between peaks area of the uniformly and non-uniformly sampled spectra.

In order to perform the second step the following operations were done: the value of the highest point of a given peak was taken and divided by two, then the peak

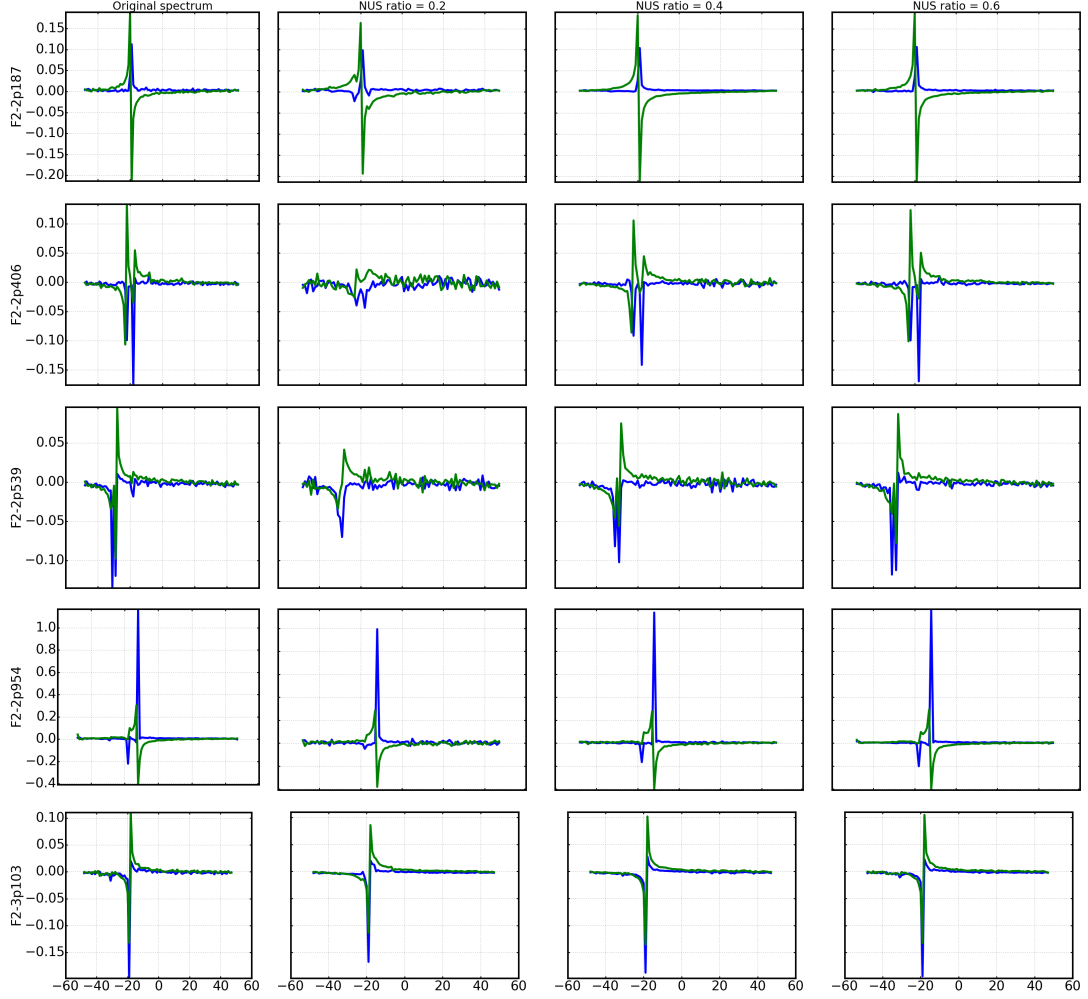


Figure 4.6: First pack of signals. Real (blue) and imaginary (green) parts of the spectrum from experimental signals. Each row is a different signal and columns (from left to right) are the original and reconstructed spectra with NUS ratio equal to 0.2, 0.4 and 0.6.

width at that height was taken and multiplied by five; that value was considered the width of the domain of the given peak. The same procedure was done for each peak. The procedure is graphically described in Figure 4.9. This procedure was only done for uniformly reconstructed spectra and same domain boundaries were applied for non-uniformly obtained spectra. The relative error for a given peak is calculated as:

$$\varepsilon_{area} = \frac{\|area_{US} - area_{NUS}\|_2}{\|area_{US}\|_2}. \quad (4.2)$$

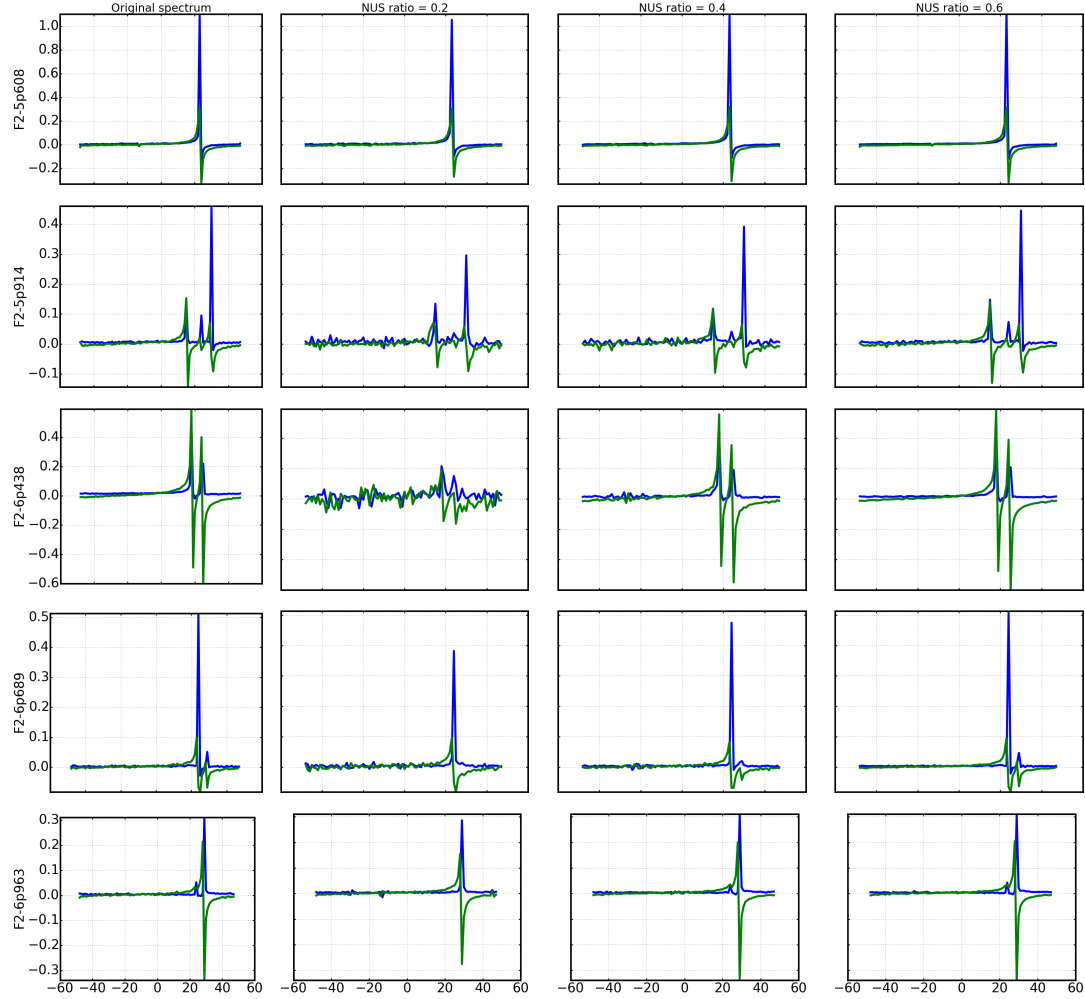


Figure 4.7: Second pack of signals. Real (blue) and imaginary (green) parts of the spectrum from experimental signals with noise. Each row is a different signal and columns (from left to right) are the original and reconstructed spectra with NUS ratio equal to 0.2, 0.4 and 0.6.

where  $area_{US}$  is the area of the peak when using uniform sampling and  $area_{UNS}$  is the area of the peak when reconstructed from non-uniformly sampled signal.

Figure 4.10 shows the results for a synthetic signal by using different  $\lambda$  and Gaussian noise standard deviation values. As it can be seen, for  $\lambda \leq 10$  higher relative errors are obtained. However, if  $\lambda$  values are greater than 10 then minimal error is achieved and no significant differences are shown for greater values. These results confirm the ones obtained in the previous section. One more important conclusion is that as noise standard deviation increases then peaks relative error increases and those with smaller area and smaller peaks are the first ones to be

affected by noise. In the rightmost figure peak 4 decreases slightly its relative error but in the opinion of the author this is just an outlier.

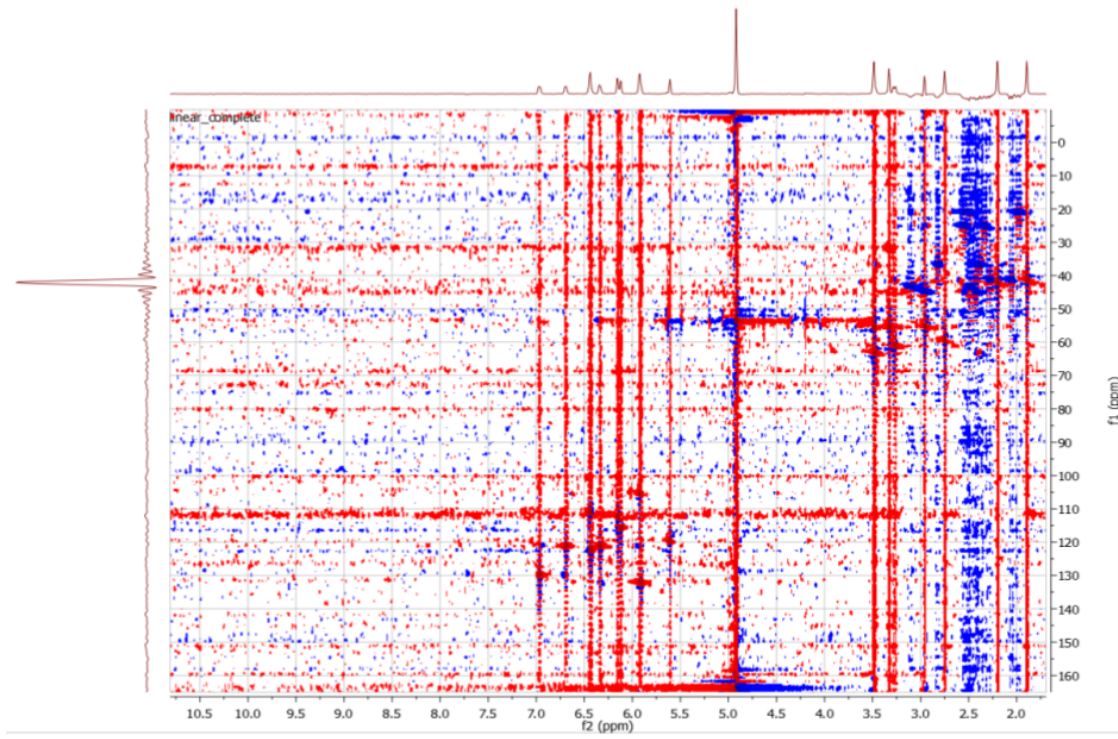


Figure 4.8: 2D spectra with two intensity thresholds from where experimental signals were taken. Blue dots indicate high content of noise.

## 4.4 Resolution of Low-Rank Reconstructed Spectrum

Another important part of the analysis is to determine how the resolution of the spectrum is affected when using different NUS ratios. It must be taken into account that if the resolution is poor then overlapping of peaks could occur which will hide many useful information for the chemist.

In order to test resolution, a noise free signal with two spectra peaks of same amplitude and decaying rate was used. At first, the two spectra peaks were separated and they were constantly moved closer in order to test how resolution was affected. In Figure 4.11 results from this experiment can be seen by using peaks at different distances. The conclusion that can be derived is that there is no significant loss of resolution when using a NUS ratio equal or greater than 0.4. However,

for a NUS ratio of 0.2 the lose of resolution is evident in cases where distance between peaks is less or equal than 0.3 frequency units.

## 4.5 Some Notes about Results Randomness Produced by Poisson-Gap Sampling

In this last section focus will be taken apart from low-rank algorithm and will be put on Poisson-gap sampling scheme. As the reader already knows, Poisson-gap sampling scheme selects sample points by following a Poisson distribution. Therefore, the sampling scheme will vary in each simulation. This implies that there exists some randomness on the results that will be obtained, that is, in each simulation similar results will be obtained but not the same. For that reason, it is interesting to analyze how results may vary by using different schemes.

Low-rank algorithm was executed 100 times in order to reconstruct F2-2.187, F2-2.406, F2-2.539, F2-2.954, F2-3.103, F2-5.608, F2-5.914, F2-6.438, F2-6.689 and F2-6.963 signals which were sampled by 100 random Poisson-gap schemes. Mean error, standard deviation and Pearson correlation between them are shown in Table 4.2. As was previously discussed there are some signals that are more difficult to reconstruct. However, it can also be seen that the ones that are harder to

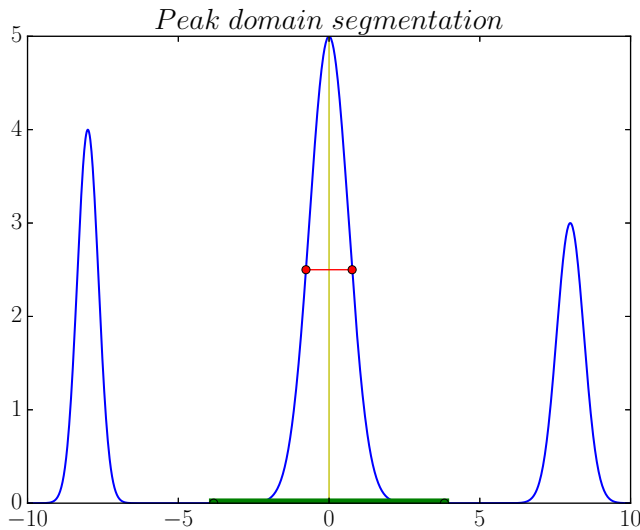


Figure 4.9: Example of peak segmentation where yellow line is the maximum height of the peak, red line is the width at half maximum height and green line is the considered domain of the peak which is five times the red line.

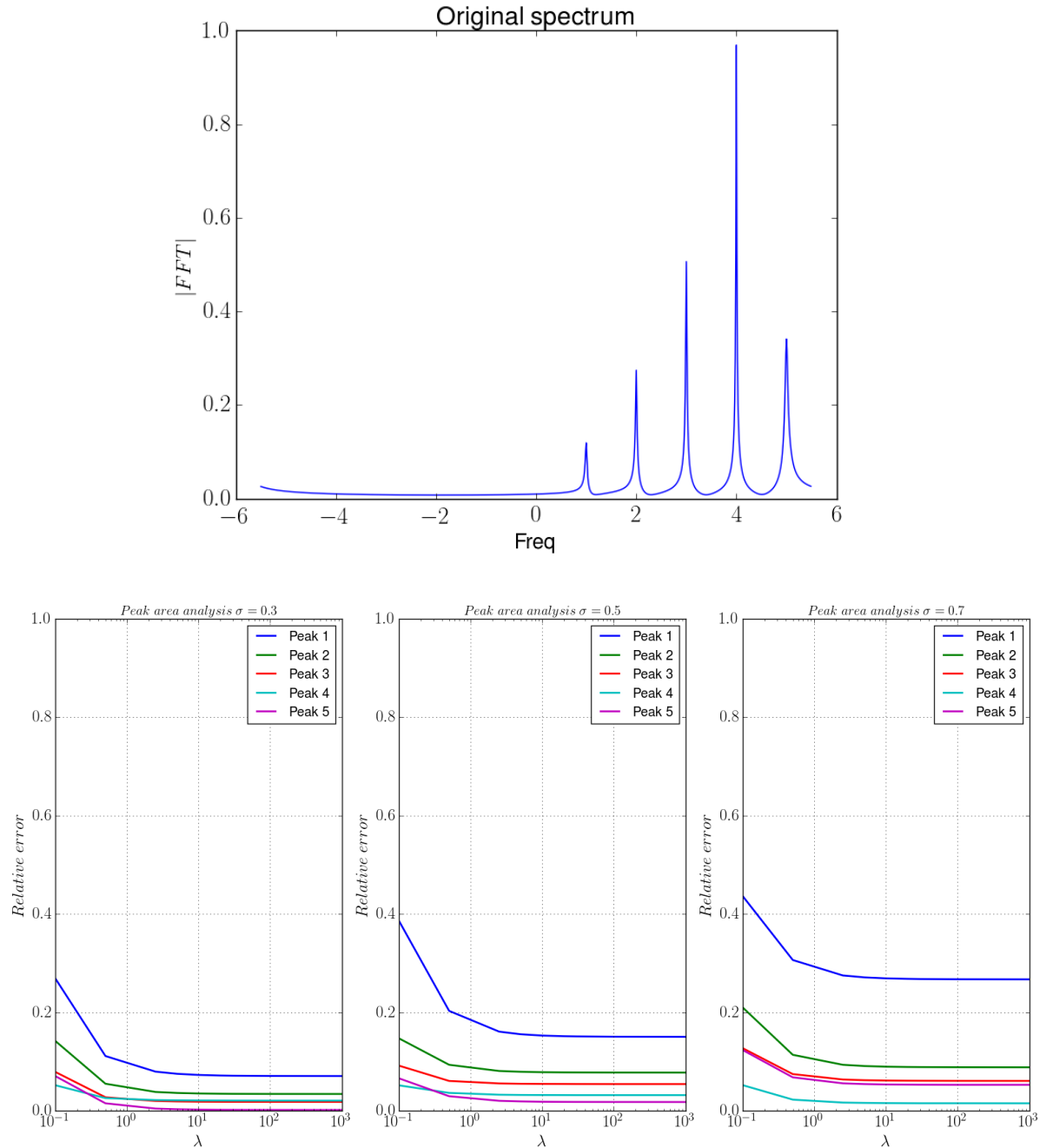


Figure 4.10: In the upper image the original synthetic spectrum can be seen where numbering of peaks is done from left to right and the area of peaks is also in increasing order from left to right. In the lower images it is shown peak area relative error for different standard deviation Gaussian noise ( $\sigma = 0.3, 0.5, 0.7$ ) and several  $\lambda$  values are shown. Minimal error is obtained for  $\lambda$  values greater than 10.

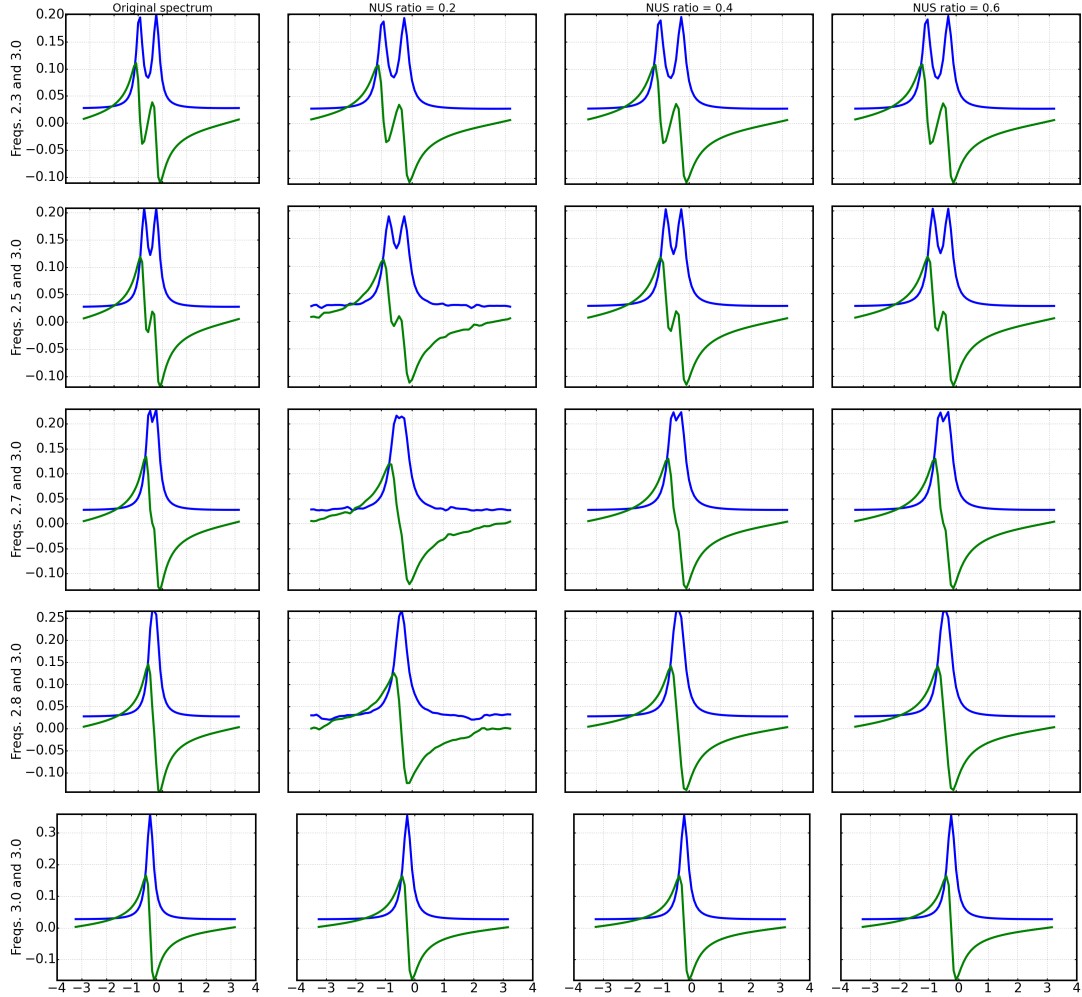


Figure 4.11: Real (blue) and imaginary (green) parts of the spectrum from resolution experiment. Each row is a different signal with frequencies at different points but with same amplitude and decaying rate. Columns (from left to right) are the original and reconstructed spectrum with NUS ratio equal to 0.2, 0.4 and 0.6.

reconstruct also have more variability in their results. In fact, as Pearson positive correlation coefficient indicates it seems that the bigger the reconstruction error the larger the results variability under different Poisson-gap sampling schemes. Moreover, Pearson correlation matrix was calculated between signals over the 100 simulation results and most correlation coefficients were near to zero. This may indicate that a specific Poisson-gap sampling scheme may succeed for one signal but not for a different one.

Signal	Mean error	Std. deviation
F2-2.187	0.0762	0.0054
F2-2.406	0.2619	0.0580
F2-2.539	0.3352	0.0538
F2-2.954	0.0784	0.0182
F2-3.103	0.1069	0.0086
F2-5.608	0.0366	0.0037
F2-5.914	0.1972	0.0311
F2-6.438	0.0663	0.0243
F2-6.689	0.0911	0.0150
F2-6.963	0.0798	0.0091
<b>Pearson Corr.</b>	<b>0.9148</b>	

Table 4.2: Mean  $L^2$  relative error and standard deviation over 100 simulations. Also Pearson correlation between mean and standard deviation is shown.



# Chapter 5

## Conclusions and Future Work

The results obtained in this master's thesis indicate that the low-rank algorithm is a suitable method for the reconstruction of Poisson-gap sampled signals. Its main advantage resides in the good balance between calculation time and the accuracy of the obtained results. For this reason, further research was done in this algorithm in order to analyze under what conditions it reconstructs optimally the signals. Special emphasis was put on  $\lambda$  and NUS ratio parameters. The results indicated that when  $\lambda \geq 10$  and NUS ratio  $\geq 0.4$  the reconstruction is going to be accurate for most signals. In fact, if the sampled signal has a small content of noise then a NUS ratio of 0.2 is sufficient. These results are quite interesting for the industry because they indicate that when sampling a two-dimensional signal at the worst case only 40 per cent of the signal must be sampled and therefore a huge save of time will be achieved. Another point to remark is that the resolution of the reconstructed spectra is almost perfect when using a NUS ratio greater or equal to 0.4. This quality decreases significantly the risk of spectrum peaks overlapping. One more important characteristic is that the peaks areas of a spectrum are not significantly perturbed in the reconstruction.

Another remarkable conclusion is that for some signals the variability of results by applying a different Poisson-gap scheme is larger than for others. In fact, the more difficult it is to reconstruct a signal, the larger the variability of the results when applying distinct Poisson-gap schemes. This results may suggest to study why for some signals the variability in the results are bigger.

About the applications of low-rank algorithm in the industry it seems that it has good perspectives. First reason is that the algorithm is quite fast for the standards of the industry, on average it spends less than one second in the reconstruction of a 96 points signal. Moreover, it can be made faster if the singular value decomposition needed to perform singular value thresholding is replaced for a more efficient method such as [9], although further research must be done because the results that are shown could not be confirmed in the practice. The second reason

for considering low-rank algorithm suitable for the industry is that the accuracy of the results outperform the results obtained from compressing sensing algorithm.

About future work, in the opinion of the author further research should be done on the presented novel method, also known as the *hybrid method*. The first task that should be performed is a research on for what type of signals hybrid method outperforms low-rank method. Then, it should also be investigated how much better are the reconstructed spectra and under what parameter values. Finally, a big effort must be done on trying to make an efficient implementation of the algorithm in order to make it applicable for industrial purposes.

# References

- [1] Convolution Theorem - Wolfram MathWorld. <http://mathworld.wolfram.com/ConvolutionTheorem.html>. Accessed: 04-07-2016.
- [2] W. P. Aue, E. Bartholdi, and R. R. Ernst. Two-Dimensional Spectroscopy. Application to Nuclear Magnetic Resonance. *Journal of Chemical Physics*, 64(5):2229–2246, 1976.
- [3] J. C. J. Barna, E. D. Laue, M. R. Mayger, J. Skilling, and S. J. P. Worrall. Exponential Sampling, an Alternative Method for Sampling in Two-Dimensional NMR Experiments. *Journal of Magnetic Resonance (1969)*, 73(1):69 – 77, 1987.
- [4] F. Bloch, W. W. Hansen, and M. Packard. The Nuclear Induction Experiment. *Phys. Rev.*, 70:474–485, Oct 1946.
- [5] S. Boyd. Alternating Direction Method of Multipliers. Video lecture: [http://videolectures.net/nipsworkshops2011\\_boyd\\_multipliers/](http://videolectures.net/nipsworkshops2011_boyd_multipliers/), 2011. [Online; accessed 27-May-2016].
- [6] S. Boyd, N. Parikh, E. Chu, B. Peleato, and J. Eckstein. Distributed Optimization and Statistical Learning via the Alternating Direction Method of Multipliers. *Found. Trends Mach. Learn.*, 3(1):1–122, January 2011.
- [7] J. F. Cai, E. J. Candès, and Z. Shen. A Singular Value Thresholding Algorithm for Matrix Completion. *SIAM J. on Optimization*, 20(4):1956–1982, March 2010.
- [8] J. F. Cai, S. Liu, and W. Xu. A Fast Algorithm for Reconstruction of Spectrally Sparse Signals in Super-Resolution. *Proc. SPIE*, 9597:95970A–95970A–7, 2015.
- [9] J. F. Cai and S. Osher. Fast Singular Value Thresholding without Singular Value Decomposition, 2010.

- [10] E. Candès, M. Wakin, and S. Boyd. Enhancing Sparsity by Reweighted  $\ell_1$  Minimization. *J. Fourier Anal. Appl.*, 14(5-6):877–905, December 2008.
- [11] E. J. Candès and B. Recht. Exact Matrix Completion via Convex Optimization. *Foundations of Computational Mathematics*, 9(6):717–772, 2009.
- [12] R. A. Chylla and J. L. Markley. Theory and Application of the Maximum Likelihood Principle to NMR Parameter Estimation of Multidimensional NMR Data. *Journal of Biomolecular NMR*, 5(3):245–258, 1995.
- [13] B. E. Coggins and P. Zhou. Polar Fourier Transforms of Radially Sampled NMR data. *Journal of Magnetic Resonance*, 182(1):84–95, September 2006.
- [14] B. E. Coggins and P. Zhou. High Resolution 4-D Spectroscopy with Sparse Concentric Shell Sampling and FFT-CLEAN. *Journal of Biomolecular NMR*, 42(4):225–239, 2008.
- [15] S. Davies, C. Bauer, P. Barker, and R. Freeman. The Dynamic Range Problem in NMR. *Journal of Magnetic Resonance (1969)*, 64(1):155 – 159, 1985.
- [16] A. J. Dingley and S. M. Pascal. *Biomolecular NMR Spectroscopy*, volume 3. IOS press, 2011.
- [17] R. Freeman. The Fourier Transform Revolution in NMR Spectroscopy. *Analytical Chemistry*, 65(17):743A–753A, 1993.
- [18] S. Hiller, I. Ibraghimov, G. Wagner, and V. Y. Orekhov. Coupled Decomposition of Four-Dimensional NOESY Spectra. *Journal of the American Chemical Society*, 131(36):12970–12978, 2009.
- [19] J. Hoch. The ABC's of NUS. [https://www.enc-conference.org/Portals/0/Tutorials/ABCs%20of%20NUS%20full%20color\\_Hoch.pdf](https://www.enc-conference.org/Portals/0/Tutorials/ABCs%20of%20NUS%20full%20color_Hoch.pdf). Accessed: 20-06-2016.
- [20] J. C. Hoch. Modern Spectrum Analysis in Nuclear Magnetic Resonance: Alternatives to the Fourier Transform. *Nuclear Magnetic Resonance Part A: Spectral Techniques and Dynamics*, 176:216 – 241, 1989.
- [21] S. G. Hyberts, H. Arthanari, S. A. Robson, and G. Wagner. Perspectives in Magnetic Resonance: NMR in the post-FFT era. *Journal of Magnetic Resonance*, 241:60 – 73, 2014. A special JMR Perspectives issue: Foresights in Biomolecular Solution-State NMR Spectroscopy From Spin Gymnastics to Structure and Dynamics.

- [22] S. G. Hyberts, H. Arthanari, and G. Wagner. Applications of Non-Uniform Sampling and Processing. *Topics in Current Chemistry*, 316:125–48, 2012.
- [23] S. G. Hyberts, G. J. Heffron, N. G. Tarragona, K. Solanky, K. A. Edmonds, H. Luithardt, J. Fejzo, M. Chorev, H. Aktas, K. Colson, K. H. Falchuk, J. A. Halperin, and G. Wagner. Ultrahigh-Resolution  $^{1}\text{H}$  $^{13}\text{C}$  HSQC Spectra of Metabolite Mixtures Using Nonlinear Sampling and Forward Maximum Entropy Reconstruction. *Journal of the American Chemical Society*, 129(16):5108–5116, 2007.
- [24] S. G. Hyberts, A. G. Milbradt, A. B. Wagner, H. Arthanari, and G. Wagner. Application of Iterative Soft Thresholding for Fast Reconstruction of NMR Data Non-Uniformly Sampled with Multidimensional Poisson Gap Scheduling. *Journal of Biomolecular NMR*, 52(4):315–327, 2012.
- [25] S. G. Hyberts, K. Takeuchi, and G. Wagner. Poisson-Gap Sampling and FM Reconstruction for Enhancing Resolution and Sensitivity of Protein NMR Data. *Journal of the American Chemical Society*, 132(7):2145–2147, 2010.
- [26] N. E. Jacobsen. *NMR Spectroscopy Explained: Simplified Theory, Applications and Examples for Organic Chemistry and Structural Biology*. Wiley, 2007.
- [27] J. Jeener. Lecture notes from Ampere Summer School in Basko Polje, Yugoslavia, September 1971.
- [28] K. Kazimierczuk, W. Komiski, and I. Zhukov. Two-Dimensional Fourier Transform of Arbitrarily Sampled NMR Datasets. *Journal of Magnetic Resonance*, 179(2):323 – 328, 2006.
- [29] K. Kazimierczuk, M. Misiak, J. Stanek, A. Zawadzka-Kazimierczuk, and W. Koźmiński. *Novel Sampling Approaches in Higher Dimensional NMR*, chapter Generalized Fourier Transform for Non-Uniform Sampled Data, pages 79–124. Springer Berlin Heidelberg, Berlin, Heidelberg, 2012.
- [30] K. Kazimierczuk and V. Y. Orehov. Accelerated NMR Spectroscopy by Using Compressed Sensing. *Angewandte Chemie International Edition*, 50(24):5556–5559, 2011.
- [31] K. Kazimierczuk, A. Zawadzka, and W. Komiski. Optimization of Random Time Domain Sampling in Multidimensional NMR. *Journal of Magnetic Resonance*, 192(1):123 – 130, 2008.

- [32] K. Kazimierczuk, A. Zawadzka-Kazimierczuk, and W. Komiski. Non-Uniform Frequency Domain for Optimal Exploitation of Non-Uniform Sampling. *Journal of Magnetic Resonance*, 205(2):286 – 292, 2010.
- [33] S. Kim and T. Szyperski. GFT NMR, a New Approach To Rapidly Obtain Precise High-Dimensional NMR Spectral Information. *Journal of the American Chemical Society*, 125(5):1385–1393, 2003.
- [34] D. E. Knuth. *The Art of Computer Programming, Volume 2 (3rd Ed.): Seminumerical Algorithms*. Addison-Wesley Longman Publishing Co., Inc., 1997.
- [35] D. M. Korzhnev, I. V. Ibraghimov, M. Billeter, and V. Y. Orekhov. MUNIN: Application of Three-Way Decomposition to the Analysis of Heteronuclear NMR Relaxation Data. *Journal of Biomolecular NMR*, 21(3):263–268, 2001.
- [36] E. Kupče and R. Freeman. Fast Reconstruction of Four-Dimensional NMR Spectra from Plane Projections. *Journal of Biomolecular NMR*, 28(4):391–395, 2004.
- [37] D. Marion. Fast Acquisition of NMR Spectra Using Fourier Transform of Non-Equispaced Data. *Journal of Biomolecular NMR*, 32(2):141–150, 2005.
- [38] O. L. Mayorga. Capítulo 8. Procesamiento de las Señales en NMR. [www.ugr.es/~olopez/estruct\\_macromol/RMN/RMN\\_13.pdf](http://www.ugr.es/~olopez/estruct_macromol/RMN/RMN_13.pdf). Accessed: 19-06-2016.
- [39] M. Mobli, J.C. Hoch, and King G.F. Fast Acquisition Methods in Multidimensional NMR. *Advances in Biomedical Spectroscopy*, 3:305–337, 2011.
- [40] M. Mobli, A. S. Stern, and J. C. Hoch. Spectral Reconstruction Methods in Fast NMR: Reduced Dimensionality, Random Sampling and Maximum Entropy. *Journal of Magnetic Resonance*, 182(1):96 – 105, 2006.
- [41] E. M. Purcell, H. C. Torrey, and R. V. Pound. Resonance Absorption by Nuclear Magnetic Moments in a Solid. *Phys. Rev.*, 69:37–38, Jan 1946.
- [42] X. Qu, M. Mayzel, J. F. Cai, Z. Chen, and V. Orekhov. Accelerated NMR Spectroscopy with Low-Rank Reconstruction. *Angewandte Chemie International Edition*, 54(3):852–854, 2015.
- [43] C. Ramirez, V. Kreinovich, and M. Argaez. Why  $\ell_1$  Is a Good Approximation to  $\ell_0$  : A Geometric Explanation. *Journal of Uncertain Systems*, 7, March 2013.

- [44] A. S. Stern, D. L. Donoho, and J. C. Hoch. NMR Data Processing using Iterative Thresholding and Minimum  $\ell_1$ -norm Reconstruction. *Journal of Magnetic Resonance*, 188(2):295–300, 2007.
- [45] V. Tugarinov, L. E. Kay, I. Ibraghimov, and V. Y. Orekhov. High-Resolution Four-Dimensional  $^1\text{H}$  $^{13}\text{C}$  NOE Spectroscopy using Methyl-TROSY, Sparse Data Acquisition, and Multidimensional Decomposition. *J. Am. Chem. Soc.*, 127(8):2767–2775, February 2005.
- [46] J. Yang and X. Yuan. Linearized Augmented Lagrangian and Alternating Direction Methods for Nuclear Norm Minimization. *Math. Comput.*, 82(281), 2013.